**Supplementary Information**

# Organocatalyzed ATRP meets nature: riboflavin-mediated synthesis of thick polymer brushes under visible light

*Justyna Bała[a,b], Anna Kiełbasa[a,b], Piotr Wieczorek[a,b], Tomasz Uchacz[a], Małgorzata Klamut[c,d], Izabela Zaborniak[c], Szczepan Zapotoczny[a], Paweł Chmielarz[c*], Karol Wolski[a*]*

[a]Faculty of Chemistry, Jagiellonian University, Gronostajowa 2, 30-387 Krakow, Poland

[b]Doctoral School of Exact and Natural Sciences, Jagiellonian University, prof. S. Lojasiewicza 11, 30-348 Krakow, Poland

[c]Department of Physical Chemistry, Rzeszow University of Technology, al. Powstancow Warszawy 6, 35-029 Rzeszow, Poland

[d]Doctoral School of the Rzeszow University of Technology, al. Powstancow Warszawy 8, 35-029 Rzeszow, Poland

*Corresponding authors: E-mail address: p_chmiel@prz.edu.pl, wolski@chemia.uj.edu.pl

# Table of Contents

## S1. Experimental

### S1.1. Materials

Unless stated otherwise, all reagents were purchased from commercial suppliers and used as received. Riboflavin (RF, 98%) was obtained from Alfa Aesar (Ward Hill, USA). Benzyl methacrylate (BzMA, stab. with ca 50-100 ppm 4-methoxyphenol, 98%) was purchased from Thermo Fischer Scientific (Waltham, USA) and passed through a column of basic alumina to remove the inhibitor before use. *α*-Bromophenylacetyl chloride (BPA-Cl, 95%) was supplied from AK Scientific (Union City, USA) and 3-(trichlorosilyl)propyl 2-bromo-2-methylpropanoate (SiClBiB) was obtained from TCI (Tokyo, Japan). (3-Aminopropyl)triethoxysilane (APTES, 99%), triethylamine (TEA, ≥99.5%), trimethylacetyl chloride (99%), ethyl *α*-bromophenylacetate (EBPA, 97%), ethyl *α*-bromoisobutyrate (EBiB, 97%), *N,N'*-dicyclohexylcarbodiimide (DCC, 99%), 4-(dimethylamino)pyridine (DMAP, 99%), *α*-bromophenylacetic acid (98%), trichlorosilane (99%), platinum(0)-1,3-divinyl-1,1,3,3-tetramethyldisiloxane complex solution, in xylene, Pt ~2% (Karstedt's catalyst solution), 5-hexen-1-ol (98%), lumichrome (LC), aluminium oxide 90 active basic (activity stage I, 0.063–0.200 mm), molecular sieves (4 Å, beads, 8-12 mesh), silica gel (high-purity grade, average pore size of 60 Å, 70-230 mesh for column chromatography), toluene (HPLC Plus, ≥99.9%), dichloromethane (DCM, p.a., ≥99.9% (GC)), *N,N*-dimethylformamide (DMF, HPLC, ≥99.9%), tetrahydrofuran (THF, HPLC, inhibitor-free, ≥99.9%), chloroform-*d* ($CDCl_3$, ≥99.8 atom% D) and dimethyl sulfoxide-$d_6$ (DMSO-$d_6$, 99.9 atom% D) were all purchased from Merck (Darmstadt, Germany). Additionally, HPLC/GC grade solvents were dried under molecular sieves prior to use in initiator grafting and polymerization experiments, as well as in photophysical measurements, when DCM was further purified by distillation before use. Methanol (p.a.), toluene (p.a.), tetrahydrofuran (THF, p.a.), *N,N*-dimethylformamide (DMF, p.a.), ethyl acetate (AcOEt, p.a.), hexane (p.a.), acetone (p.a.), magnesium sulphate ($MgSO_4$, anhydrous pure p.a.) and hydrofluoric acid (HF, 40%, p.a.) were received from Chempur (Piekary Śląskie, Poland). Dichloromethane (DCM) and ethanol (96%, p.a.) were obtained from Stanlab (Lublin, Poland) and *N*-methyl-2-pyrrolidinone (NMP, 99.8%) was purchased from Fluorochem (Glossop, UK). Silicon wafers were supplied by ON Semiconductor (Roznov, Czech Republic).

## S1.2. Methods

Atomic Force Microscopy (AFM) images were captured using a Dimension Icon AFM (Bruker, Santa Barbara, CA, USA) operated in the PeakForceTapping (PFT) and QNM® modes. The standard silicon cantilevers for measurements in the air (nominal spring constant of 0.4 N $m^{-1}$) were used. To determine the thickness of the brush, the polymer layers were scratched with a needle, and measurements were taken at the formed edge. Raw data were converted into topography images using NanoScope Analysis 1.9 software. AFM images were subjected to standard processing, including plane fit and flattening procedure (line-by-line correction). In the case of height measurements, the scratched surface area was levelled to 0 nm on the z-scale, allowing for a visual comparison of layer thickness, particularly when AFM images are presented on the same Z scale. To eliminate other artefacts, the horizontal line erase function was applied. For each sample, several micrographs at different places were captured, and the thicknesses of the polymer brushes were determined from the height histograms and reported as averages.

Fourier transform infrared (FTIR) spectra were recorded using a Nicolet iS10 spectrometer equipped with an MCT/A detector (Thermo Fisher Scientific, Waltham, MA, USA) and an ATR accessory (Smart iTX) at a resolution of 4 $cm^{-1}$. Each spectrum represents an average of 128 scans and was baseline-corrected using Omnic software.

Nuclear magnetic resonance (NMR) spectra were recorded using Jeol High-field (400 MHz and 600 MHz) in $CDCl_3$ or DMSO-$d_6$. Chemical shifts ($\delta$) were reported in ppm and analyzed in reference to the solvent residual signal.

The ToF–SIMS experiments were performed on an IONTOF ToF-SIMS V (Munster, Germany) instrument, equipped with a bismuth–manganese liquid metal ion source. The powder of the sample was sticked to the substrate with the carbon tape. Surface composition was measured with $Bi_3$ ion beam (0.5 pA) rastered over 250 µm × 250 µm. The analysis time was adjusted to keep the dose density below the static limit for organics (dose density 2.45 × $10^{11}$ ion $cm^{-2}$). Mass calibration for positive spectra was done with $H^+$, $H_2^+$ $CH^+$, $C_2H^+$ $C_2H_2^+$, $C_4H_4^+$, $C_5H_5^+$. Mass spectra were analyzed with IonTOF SurfaceLab 7.3 software.

Variable-Angle Spectroscopic Ellipsometry (VASE) measurements were performed on the M200U spectroscopic ellipsometer (J. A. Wollam, USA). The thickness of the polymer brushes was evaluated as the arithmetic means of two measurements at different locations. Raw data

was then fitted to the basis of the Cauchy model using the CompleteEASE software. Depending on the polymer layer thickness, the range was switched from 550-1000 nm to 360-1000 nm.

UV-Vis absorption spectra were recorded in quartz cuvettes (Hellma, 10 mm path length) at room temperature under anaerobic conditions using a Hitachi U-2900 dual-beam spectrophotometer and a Cary 60 UV−Vis spectrophotometer (Agilent Technologies). Spectra were recorded with the adjusted parameters, respectively: for the Hitachi U-2900, a scan speed of 800 nm $min^{-1}$ with a 10 nm optical path correction relative to the corresponding baseline and then smoothed with a Savitzky-Golay filter and for the Cary 60, scan speed of 600 nm $min^{-1}$, baseline-corrected against the solvent. All spectra were acquired with a data interval of 1.0 nm.

Fluorescence spectra were recorded in quartz cuvettes (Hellma, 10 mm path length) at room temperature, while phosphorescence and luminescence spectra at -196°C using a Hitachi F-7000 spectrofluorometer. The spectra were collected at a scan rate of 240 nm $min^{-1}$ with the excitation and emission slits set at 2.5 nm and the photomultiplier voltage at 800 V. All spectra were acquired at an excitation of 440 nm, corrected for the photomultiplier sensitivity curve and smoothed.

Lifetimes of the excited states were determined using a picosecond UV-VIS-NIR Fluorolog 3 spectrofluorometer (Horiba Jobin Yvon) equipped with a TCSPC (time-correlated single photon counting) detector and NanoLED-460 light source (λ peak = 464 nm, 7 pJ/pulse). A light-scattering Ludox solution was used to acquire the instrument-response function, and an exponential function was fitted to the emission decay curves.

Gel permeation chromatography (GPC) was performed using a Shimadzu (Kyoto, Japan) modular system consisting of a CBM-40 system controller, SIL-20AHT automatic injector, RID-20A differential refractive-index detector, and CTO-20A column oven (the temperature was maintained at 35°C). Analyses were performed using Dr Maisch's combination columns made of stainless steel (V4A). The column set consisted of a precolumn and three Repro-Gel 5 µm columns (500 Å, 10 000 Å, and 100 000 Å). To determine the molecular weights ($\overline{M}_n$) and molecular weight distributions (Đ) of degrafted polymer chains from the planar surface, tetrahydrofuran (HPLC grade) was used as an eluent in chromatographic separation; *N,N*-dimethylformamide (HPLC grade, with 0.01 M LiCl) was used for the characterization of polymers synthesized in solution. The flow rate was set at 1 mL $min^{-1}$. Calibration was performed with commercial PMMA standards with narrow molecular weight distribution (PSS Polymer).

## S1.3. Procedures

### S1.3.1. Synthesis of BPA-based surface-tethered initiator

Synthesis of 6-(trichlorosilyl)hexyl 2-bromo-2-phenylacetate (SiClBPA) was conducted in a two-step modified procedure presented by Matyjaszewski's group.[1] In a 500 mL three-necked round-bottom flask 5-hexen-1-ol (6.8 mL, 57 mmol), $\alpha$-bromophenylacetic acid (10 g, 47 mmol) and DMAP (0.51 g, 4.2 mmol) were dissolved in distilled DCM (134 mL). The reaction mixture was stirred and cooled down in an ice bath. The solution of DCC (10.7 g, 52 mmol) in DCM (40 mL) was prepared and also chilled in ice. After that, it was slowly added over 1.5 h, keeping the temperature below 0°C. The reaction was left to proceed for 24 h at room temperature. After completion, the product was filtered and the precipitate was washed with DCM. Solvent was evaporated under reduced pressure, and the obtained product was purified by column chromatography eluted with a mixture of hexane/ethyl acetate (30/1 v/v). The final product of hex-5-en-1-yl 2-bromo-2-phenylacetate was a faint yellow liquid (10.39 g, 62%).

**$^1$H NMR** (400 MHz $CDCl_3$, **Figure S1**): ***δ*** (ppm) 7.56 (m, 2H, Ar), 7.35 (m, 3H, Ar), 7.26 ($CDCl_3$), 5.75 (ddt, 1H, $CH_2$=C**H**-), 5.35 (s, 1H, -**H**C-Ar), 4.97 (m, 2H, C**H$_2$**=CH-), 4.19 (quint, 2H,-C**H$_2$**-OC=O), 2.06 (q, 2H,$CH_2$=CH-C**H$_2$**-), 1.65 (m, 2H, $CH_2$=$CHCH_2CH_2$-C**H$_2$**-), 1.42 (m, 2H, $CH_2$=$CHCH_2$-C**H$_2$**-). **$^{13}$C NMR** (101 MHz, $CDCl_3$, **Figure S2**): ***δ*** (ppm) 168.4 (-O-**C**=O), 138.3 ($CH_2$=**C**H-), 136.0, 129.4, 128.9, 128.8 (Ar), 115.0 (**C**$H_2$=CH-), 77.2 ($CDCl_3$), 66.4 (-**C**$H_2$-OC=O), 47.0 (-**C**H-Ar), 33.2 ($CH_2$=CH-**C**$H_2$-), 27.9 ($CH_2$=$CHCH_2CH_2$-**C**$H_2$-), 25.0 ($CH_2$=$CHCH_2$-**C**$H_2$-). See also FTIR spectrum (**Figure S3**) with analysis of bands (**Table S1**).

Hex-5-en-1-yl 2-bromo-2-phenylacetate (6.54 g, 22 mmol) was mixed with trichlorosilane (4.44 mL, 44 mmol). The solution was placed in an ice bath and purged with dry nitrogen for 5 min. After that, the Karstedt's catalyst solution (0.2 mL) was injected to the reaction mixture. The reaction was continued at room temperature under constant stirring for 5 days. An excess of trichlorosilane was removed under reduced pressure. The reaction proceeded quantitatively, yielding the product as a yellow liquid.

**$^1$H NMR** (400 MHz, $CDCl_3$, **Figure S4**): ***δ*** (ppm) 7.55 (m, 2H, Ar), 7.36 (m, 3H, Ar), 7.25 ($CDCl_3$), 5.35 (s, 1H,-**H**C-Ar), 4.18 (t, 2H, -C**H$_2$**-O), 1.76-1.50, 1.36 (m, 10H, $Cl_3SiC$**H$_2$C H$_2$C H$_2$C H$_2$C H$_2$**-). **$^{13}$C NMR** (101 MHz, $CDCl_3$, **Figure S5**): ***δ*** (ppm) 168.7 (-O-**C**=O), 135.9, 129.4, 128.9, 128.7 (Ar), 77.2 ($CDCl_3$), 66.4 (-**C**$H_2$-OC=O), 47.0 (-**C**H-Ar), 31.3 ($Cl_3SiCH_2CH_2CH_2$**C**$H_2$-), 28.2 ($Cl_3SiCH_2CH_2$**C**$H_2$-), 25.2 ($Cl_3SiCH_2CH_2CH_2CH_2$**C**$H_2$-), 24.2

($Cl_3SiCH_2\mathbf{C}H_2$-), 22.2 ($Cl_3Si\mathbf{C}H_2$-). See also FTIR spectrum (**Figure S6**) with analysis of IR bands (**Table S2**).

### S1.3.2. Preparation of the modified riboflavin (modRF)

Acylation of riboflavin was performed according to the modified procedure reported in the literature.[2] All operations were performed in the dark. In a 100 mL three-necked round-bottom flask under anaerobic conditions, riboflavin (1 g, 2.66 mmol) was dissolved in NMP (23.34 mL) with the addition of TEA (1.48 mL, 10.61 mmol). The mixture was placed in an ice bath and a solution of trimethylacetyl chloride (3.92 mL, 31.83 mmol) in NMP (17.34 mL) was added dropwise over 3 h while maintaining the reaction temperature below 0°C. Then, the reaction mixture was stirred over 7 days at room temperature. After completion, the product was dissolved in DCM (25 mL) and washed with water (42 mL × 15), then dried over anhydrous $MgSO_4$. Combined organic phases were concentrated in vacuo. The obtained crude material was purified by column chromatography using a gradient eluent system, from pure DCM to DCM/MeOH (95/5 v/v) to get the final product – modRF as an orange powder (0.85 g; 45%). **$^1$H NMR** (400 MHz, $CDCl_3$, **Figure S7**): ***δ*** (ppm) 8.73 (s, 1H, NH), 8.02 (s, 1H, =CH-), 7.83-7.59 (d, J=96.6 Hz, 1H, =CH-), 7.25 ($CDCl_3$), 5.38 (m, 2H, -$CH_2$-), 4.90 (m, 2H, -CH-), 4.53 (m, 1H, -CH-), 4.17 (m, 2H, -$CH_2$-), 2.55-2.51 (d, J=13.7 Hz, 3H, -$CH_3$), 2.42 (s, 3H, -$CH_3$), 1.28 - 0.92 (33H, -$CH_3$). **$^{13}$C NMR** (151 MHz, DMSO-*d*$_6$, **Figure S8**): ***δ*** (ppm) 177.3-176.3 (4C, -O-C=O), 159.9 (2C, -C=O), 155.4 (2C, -C=N-), 146.7 (1C, -C=C-), 136.8-133.9 (5C, -C=C-), 71.4 (1C, -CH-), 70.1 (1C, -CH-), 67.5 (1C, -CH-), 62.5 (2C, -$CH_2$-), 39.7 (DMSO-*d*$_6$), 38.6-38.2 (4C, -**C**($CH_3$)$_3$), 27.0-26.9 (12C,-C(**C**$H_3$)$_3$), 21.0 (1C, -$CH_3$), 18.9 (1C, -$CH_3$). **ToF SIMS** (**Figure S9**): $[M+H]^+$ 713.4386 ($C_{37}H_{53}N_4O_{10}^+$). FTIR spectra are presented in **Figure S10**, and the analysis of the IR bands is given in **Table S3** and **Table S4**.

### S1.3.3. Photophysical measurements

Photophysical measurements were carried out in the dark to avoid unintentional irradiation of the photocatalyst solutions and all samples were purged with argon prior to analysis. Assays were conducted in DMF (HPLC grade, ≥99.9%), which was dried over molecular sieves before use to best reproduce the polymerization conditions. Additionally, acetone was filtered through a 0.45 μm hydrophobic PTFE syringe filter. Fluorescence quantum yield of the obtained photocatalyst (modRF) was determined using riboflavin as a standard, based on the equation 1:[3]

$$\varphi_{fl} = \varphi_0 \frac{I_s}{I_r} \times \frac{OD_r}{OD_s} \times \left(\frac{n_s}{n_r}\right)^2 \quad (1)$$

where $\varphi_0$ is the known quantum yield of RF in acetone ($\varphi_0$ = 0.36),[4] $I$ is the integrated fluorescence intensity, *OD* is the optical density and *n* represents the solvent refractive index (1.4305 for DMF and 1.3586 for acetone). The subscript *r* refers to the reference (RF) and *s* to the sample (modRF).

### S1.3.4. ATRP initiators grafting

Silicon wafers were cleaned by rinsing with ethanol and then ultrasonicated in ethanol for 10 min at 50°C. Dried substrates were treated using UV Ozone cleaning (Ossila, Sheffield, UK) for 30 min. Three types of surface-tethered initiators were grafted onto the wafers according to the following procedures.

*SiClBiB functionalization:* procedure was adapted from our earlier work[5] with slight modifications. TEA (30 µL) was added slowly to the conical flask containing cleaned substrates immersed in dried toluene (20 mL) under an Ar atmosphere. After 10 min of inert gas bubbling, SiClBiB (5 µL) was added dropwise to the mixture. The reaction was left to proceed for at least 20 h. Then the silicon wafers were rinsed with toluene, placed in an ultrasonication bath for 1 min in pulse mode in the same solvent and washed sequentially with toluene, DCM, toluene and finally dried in the stream of nitrogen.

*APTES-BPA functionalization:* immobilization was performed based on the method reported previously by our team.[6]

*SiClBPA functionalization:* the synthesized initiator was used to create an initiator monolayer, similarly to the approach presented in the procedure with SiClBiB. Substrates were placed in dried toluene (19.5 mL) with TEA (30 µL), purged with Ar. Then the 0.5 mL solution of SiClBPA initiator in toluene (10 µL $mL^{-1}$) was added to the mixture. After at least 20 h, the silicon wafers were washed as described above for SiClBiB functionalization.

### S1.3.5. Surface-Initiated Organocatalyzed Atom Transfer Radical Polymerization (SI-O-ATRP) of benzyl methacrylate

SI-O-ATRP polymerizations were performed in one batch simultaneously from three silicon wafers functionalized with all types of initiators. All operations were carried out in the dark. Stock solutions of PC were prepared in dried DMF and stored under Ar atmosphere. In the case of RF molar concentration was set to 66.4 µM by dissolving 3 mg of RF (7.97 µmol) in DMF (120 mL) by ultrasonication. Thanks to the higher solubility of modRF, the stock solution with

a higher molar concentration (140 μM) was obtained by adding 2 mg of modRF (2.81 μmol) to DMF (20 mL). The polymerization setup consisted of three bottles sealed with rubber septa and connected *via* double-tipped needles. The last bottle contained initiator-functionalized silicon wafers placed in a custom-made holder to enable stirring, immersed in 1 mL of BzMA (5.90 mmol). The bottle was installed on a 3 cm stand on the magnetic stirrer. The middle vial was filled with PC solution: (1) 1 mL of RF (0.066 μmol) stock solution or (2) 0.473 mL of modRF (0.066 μmol) stock solution combined with 0.527 mL of dried DMF. The first bottle was charged with pure solvent to saturate the system with DMF vapors. After 30 min of Ar purging, the PC solution was transferred *via* cannula to the third bottle. The final polymerization mixture was stirred and reagents ratios were 50/50 v/v BzMA/DMF and [BzMA]/[PC]: 1/0.000011 (molar ratio) (11 ppm of PC). Once the homogenous solution was obtained, the LED reactor ($\lambda_{max}$ = 450 nm) was positioned on 3.5 cm high supports, and irradiation was started. Intensity of the used light was set to (95 ± 5) W $m^{-2}$. Images of the experimental setup are presented in **Figure S11**. After completion, the polymerization was stopped by removing the light source and opening the bottle. Silicon wafers with synthesized PBzMA nanobrushes were cleaned by rinsing with a sequence of organic solvents: DMF, THF, toluene and dried in the stream of nitrogen. In case of other PC and different concentrations, following stock solutions and compositions of second bottle were prepared (the volume ratio of monomer to solvent was kept constant 50/50 v/v BzMA/DMF): for [BzMA]/[modRF]: 1/0.0000622 (62 ppm modRF) – 0.052 mL of stock solution (7 mM) mixed with 0.948 mL of DMF; [BzMA]/[modRF]: 1/0.000625 (625 ppm of modRF) – 0.526 mL of stock solution (7 mM) mixed with 0.474 mL of DMF; [BzMA]/[LC]: 1/0.000011 (11 ppm of LC) – 0.214 mL of stock solution (0.31 mM) mixed with 0.786 mL of DMF; [BzMA]/[LC]: 1/0.000112 (112 ppm of LC) – 0.321 mL of stock solution (2.1 mM) mixed with 0.679 mL of DMF.

### S1.3.6. Cleaving polymer brushes from the substrate

To obtain significant amounts of polymer material from the substrate to conduct GPC analysis, synthesis of PBzMA nanobrushes was performed on a large silicon wafer (Ø 10 cm). The polymerization solution was prepared as described in the previous procedure, maintaining the molar ratios of all reactants (50/50 v/v BzMA/DMF; [BzMA]/[modRF]: 1/0.000011; 11 ppm of modRF) with the increased total volume to 40 mL. Then, inside the glovebox, a mixture was poured onto the SiClBPA modified substrate, placed in a glass jar. The vessel was sealed using a glass lid, protected by Parafilm, removed from the glovebox and then installed on an orbital shaker to ensure proper mixing during light exposure. Polymerization was conducted for 8

hours, and the plate was then washed in the same manner as for small scale synthesis. Cleaving of the characterized PBzMa brush was performed based on the modified approach reported by Klok et al.[7] The silicon wafer was cut into smaller pieces to fit into a PTFE evaporating dish containing THF (HPLC grade, 29.7 mL) and HF (0.3 mL of 40% HF). The mixture was left at room temperature under a fumehood for 2 h. After that, the plates were gently rinsed with THF above the Teflon container to avoid polymeric material loss. The residues with detached PBzMA chains were allowed to evaporate to dryness for 48 h at 40°C. Then, the obtained polymer was redissolved in 7.5 mL of THF and transferred to a small bottle. The vessel was left for 3 days under a working fume and the sample was finally dried in a vacuum dryer at 40°C. The polymer material was analyzed by GPC chromatography.

**S1.3.7. O-ATRP of benzyl methacrylate in solution**

Preparation of PBzMA in solution was carried out analogously to the synthesis from the surface. Pure DMF was placed in the first vial to saturate the polymerization setup with the solvent vapors. In the second bottle, a given amount of BzMA (1 mL) was mixed with a proper amount of PC stock solution (volumes selected for appropriate concentrations). The last vessel contained a stock solution of sacrificial initiator in DMF (0.108 mL of 68.1 mM EBiB solution or 0.129 mL of 57.1 mM EBPA solution) with DMF (appropriate volumes reduced by the solvent already present in the initiator solution). Before irradiation, the initial sample was taken *via* syringe and during polymerization, the samples were withdrawn periodically to follow the polymerization kinetics. Monomer conversion was monitored by $^{1}$H NMR measurements, while GPC was used to characterize $\bar{M}_n$ and Đ of the formed polymer.

## S2. Characterization of synthesized BPA-based surface-tethered initiator

### S2.1. Characterization of hex-5-en-1-yl 2-bromo-2-phenylacetate

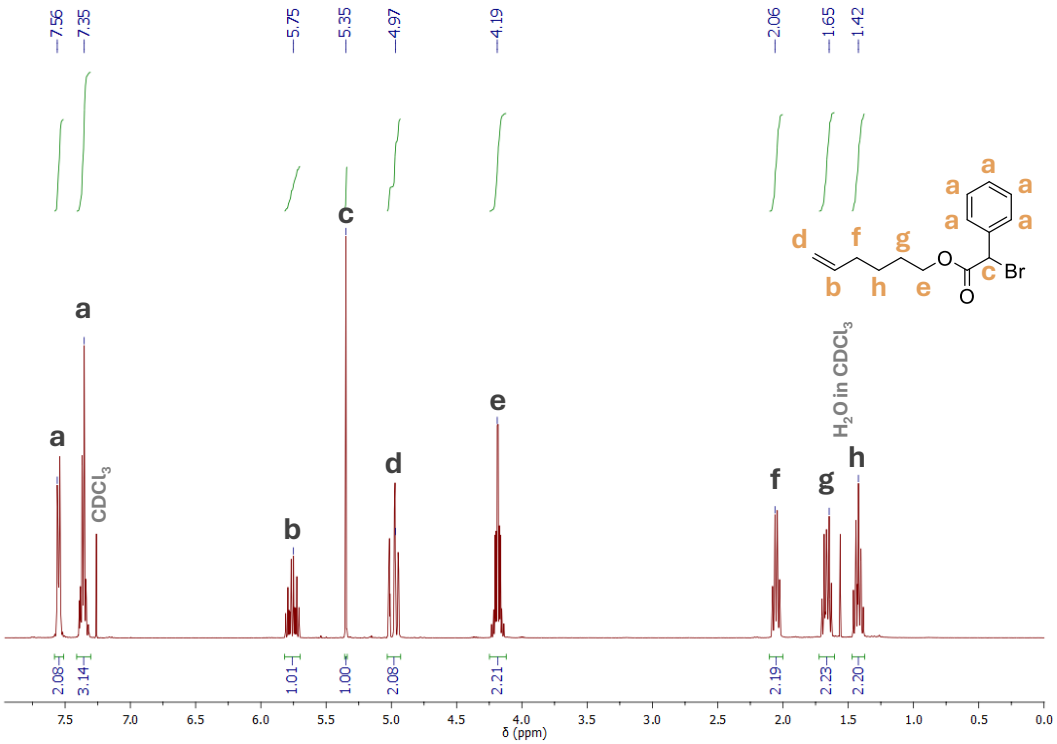


**Figure S1**. $^{1}$H NMR ($CDCl_3$) spectrum of hex-5-en-1-yl 2-bromo-2-phenylacetate.

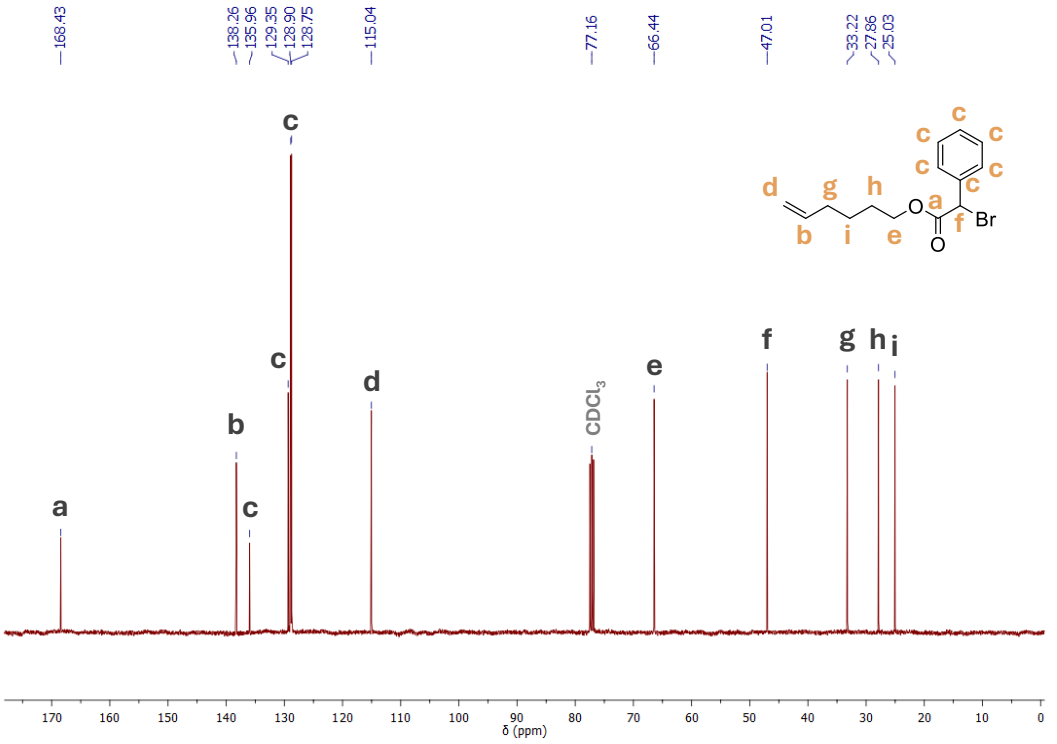


**Figure S2**. $^{13}$C NMR ($CDCl_3$) spectrum of hex-5-en-1-yl 2-bromo-2-phenylacetate.

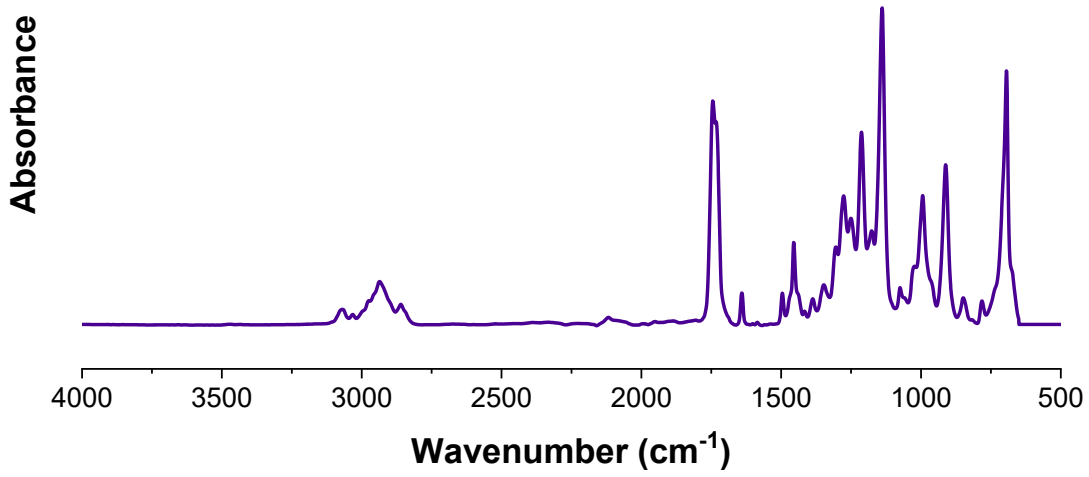


**Figure S3**. FTIR spectrum of hex-5-en-1-yl 2-bromo-2-phenylacetate.

**Table S1**. Analysis of the FTIR spectrum of hex-5-en-1-yl 2-bromo-2-phenylacetate demonstrated in **Figure S3**.

| **Major IR band wavenumber ($cm^{-1}$)** | **Characteristics and assigned vibrations** |
|---|---|
| 3075 | Ar-H stretching<br>C-H stretching from $RCH=CH_2$ |
| 2937<br>2862 | C-H stretching from $C-CH_2-C$ |
| 1745 | C=O stretching from ester group |
| 1641 | C=C stretching from $RCH=CH_2$ |
| 1496 | C–C stretching from monosubstituted ring |
| 1456 | $C-CH_2$ symmetrical deformations |
| 1213 | C-O stretching from ester group |
| 1139 | C-O stretching from ester group |
| 995 | C-H bending from $RCH=CH_2$ |
| 913 | C-H bending from $RCH=CH_2$ |

## S2.2. Characterization of 6-(trichlorosilyl)hexyl 2-bromo-2-phenylacetate

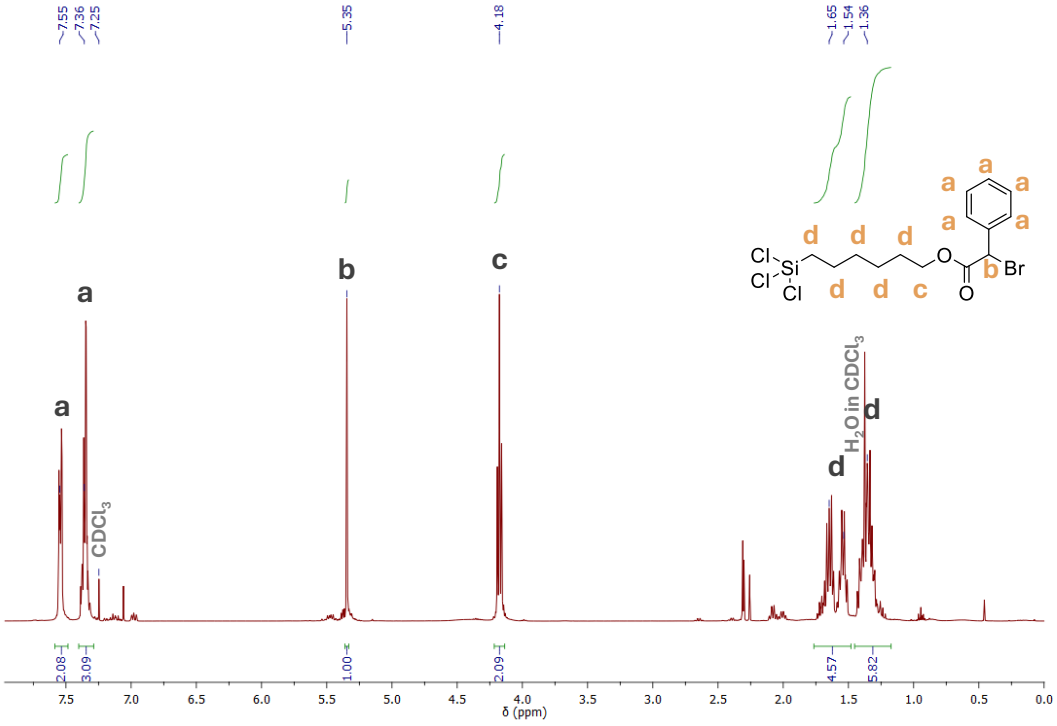


**Figure S4**. $^{1}$H NMR ($CDCl_3$) spectrum of 6-(trichlorosilyl)hexyl 2-bromo-2-phenylacetate.

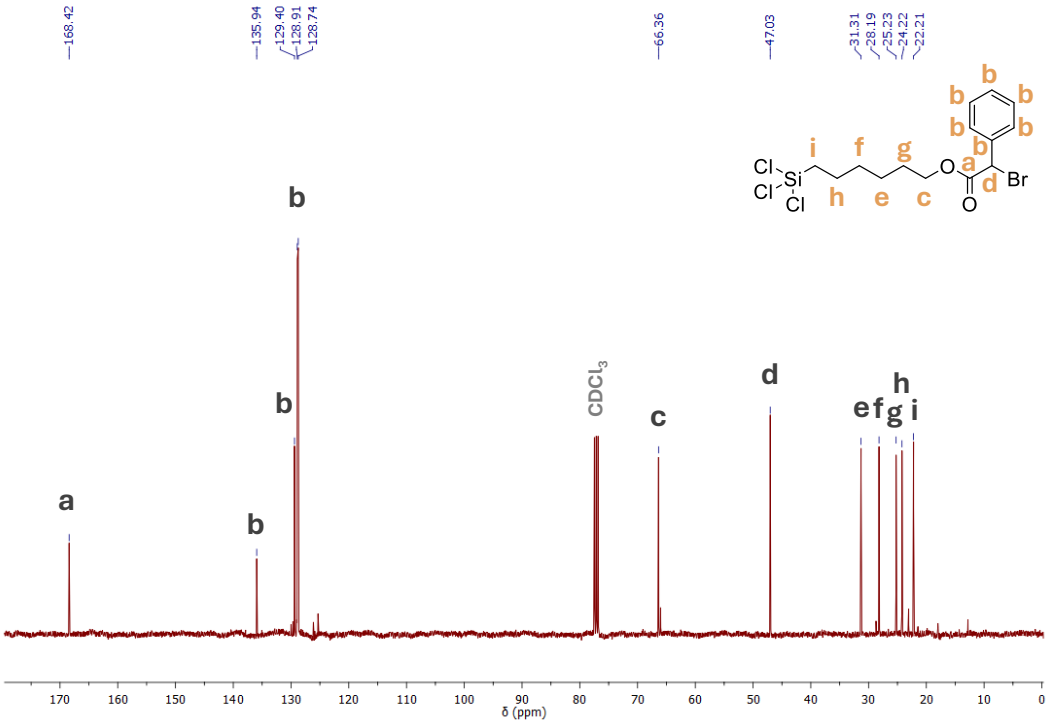


**Figure S5**. $^{13}$C NMR ($CDCl_3$) spectrum of 6-(trichlorosilyl)hexyl 2-bromo-2-phenylacetate.

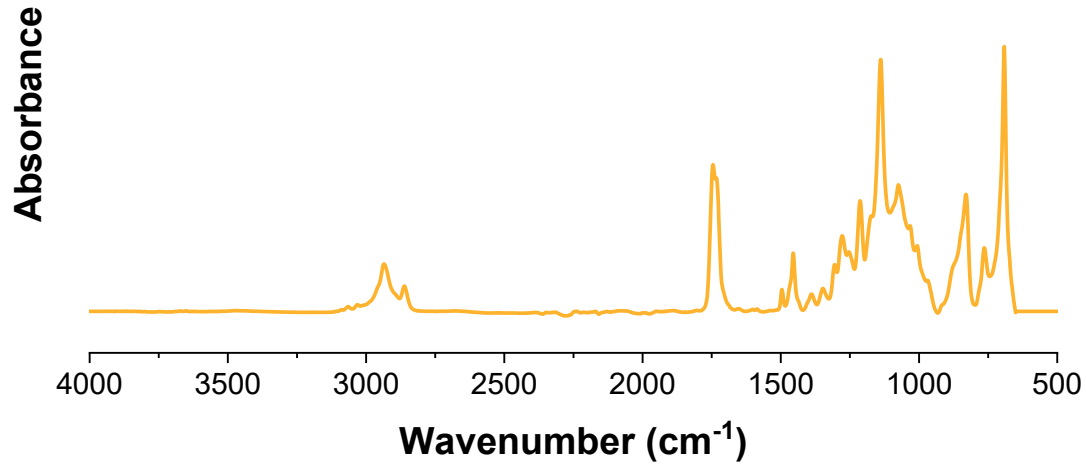


**Figure S6**. FTIR spectrum of 6-(trichlorosilyl)hexyl 2-bromo-2-phenylacetate.

**Table S2**. Analysis of the FTIR spectrum of 6-(trichlorosilyl)hexyl 2-bromo-2-phenylacetate demonstrated in **Figure S6**.

| **Major IR band wavenumber ($cm^{-1}$)** | **Characteristics and assigned vibrations** |
|---|---|
| 3075 | Ar-H stretching |
| 3034 | C-H stretching from aromatic ring |
| 2937 | C-H stretching from C-$CH_2$-C |
| 2864 | |
| 1745 | C=O stretching from ester group |
| 1733 | |
| 1496 | C-C stretching from monosubstituted ring |
| 1456 | C-$CH_2$ symmetrical deformations |
| 1213 | C-O stretching from ester group |
| 1139 | C-O stretching from ester group |

## S3. Preparation of the modified riboflavin – characterization of obtained product: acylated riboflavin (modRF)

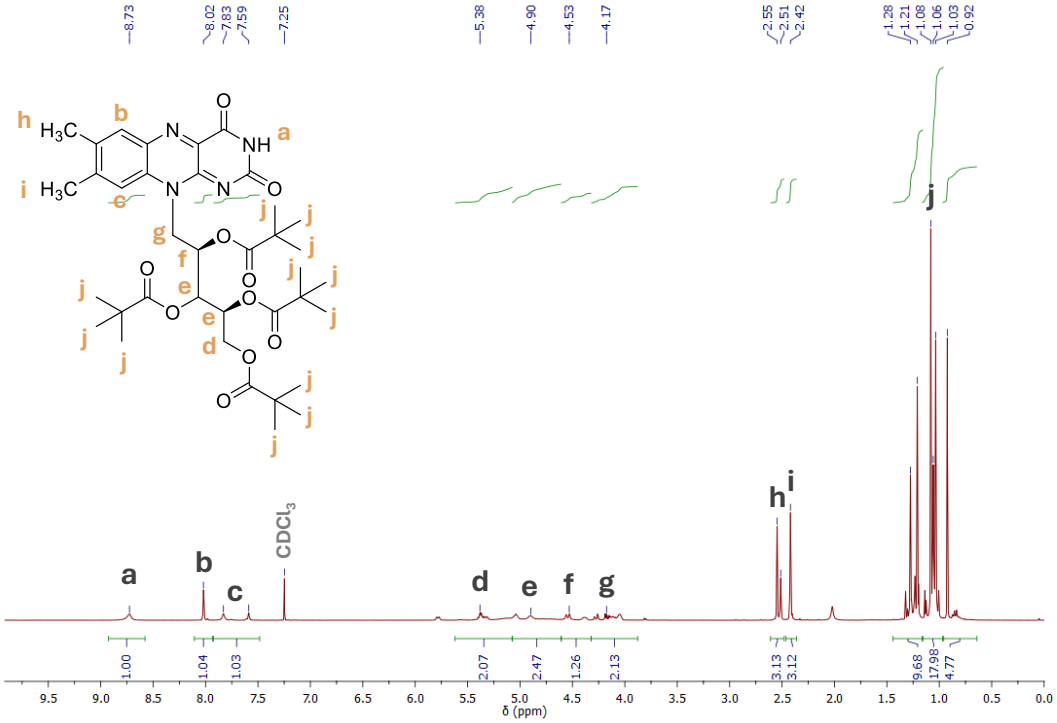


**Figure S7**. $^{1}$H NMR ($CDCl_3$) spectrum of synthesized modRF.

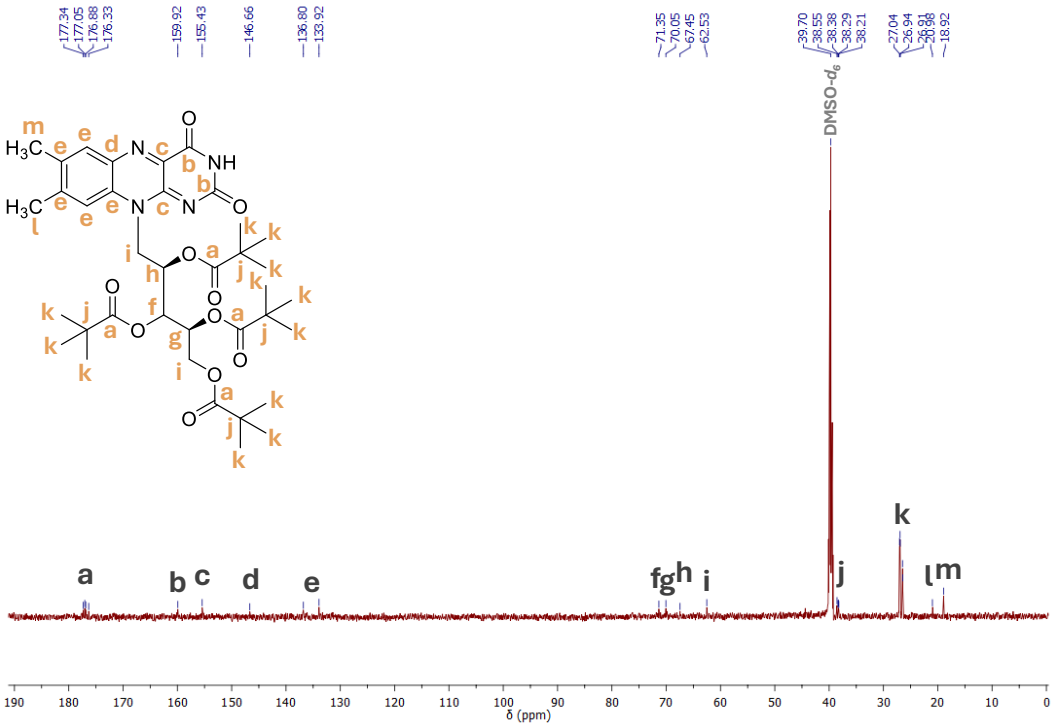


**Figure S8**. $^{13}$C NMR (DMSO-$d_6$) spectrum of synthesized modRF.

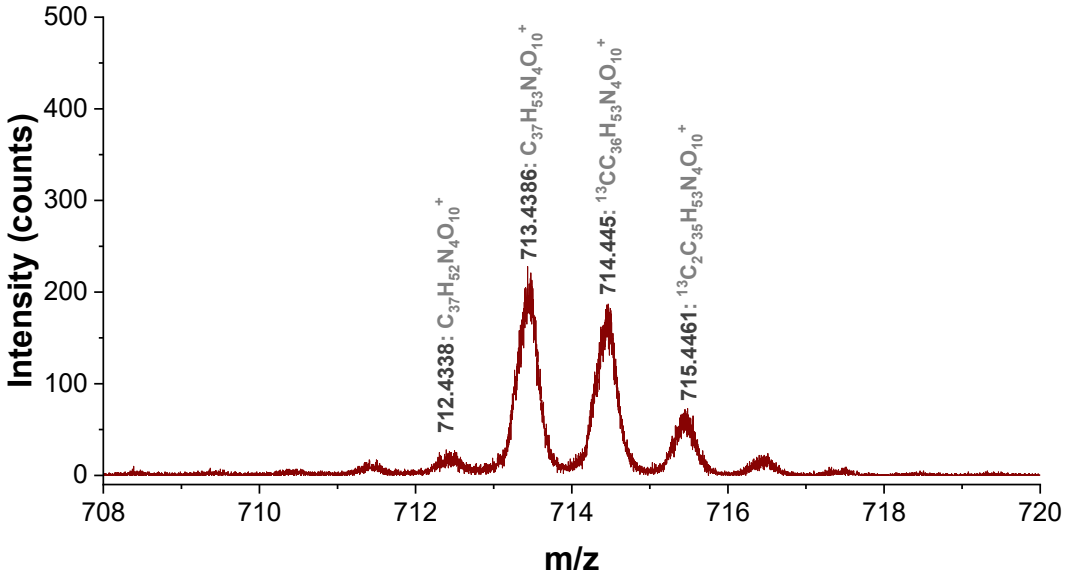


**Figure S9**. ToF-SIMS spectrum of modRF.

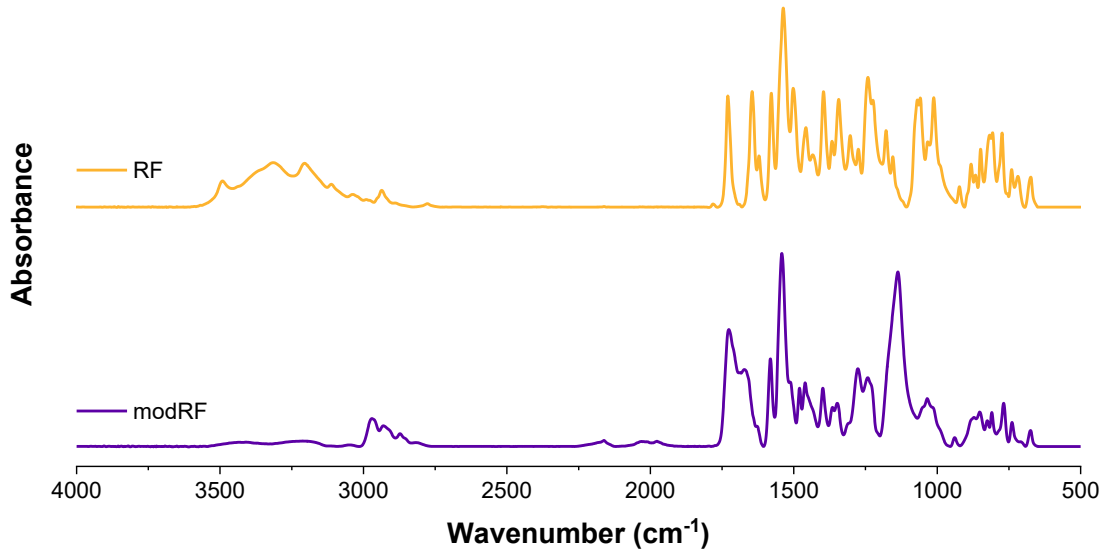


**Figure S10**. FTIR spectra of riboflavin (RF) and acylated riboflavin (modRF).

**Table S3**. Analysis of the FTIR spectrum of RF demonstrated in **Figure S10**.

| **Riboflavin (RF)** | |
|---|---|
| **Major IR band wavenumber ($cm^{-1}$)** | **Characteristics and assigned vibrations** |
| 3490 | N-H stretching from imide group |
| 3318 | O-H stretching and possibly intramolecular hydrogen bonded –OH groups |
| 3110<br>3038 | =C-H stretching from aromatics |
| 2937 | C-H stretching from methyl groups on aromatic ring |
| 1730 | C=O stretching from imide group |
| 1645 | C=C stretching from aromatics |
| 1577 | N-H bending |
| 1539 | C=N stretching |
| 1061 | C-OH stretching from ribitol tail |

**Table S4**. Analysis of the FTIR spectrum of synthesized modRF demonstrated in **Figure S10**.

| **Acylated riboflavin (modRF)** | |
|---|---|
| **Major IR band wavenumber ($cm^{-1}$)** | **Characteristics and assigned vibrations** |
| 3445 | N-H stretching from imide group |
| 3051 | =C-H stretching from aromatics |
| 2970 | C-$CH_3$ stretching from *tert*-butyl groups |
| 2930 | C-$CH_2$-C stretching from aliphatic groups |
| 2873 | C-H stretching from methyl groups on aromatic ring |
| 1730 | C=O stretching from imide group |
| 1672 | C=O stretching from ester groups |
| 1583 | N-H bending |
| 1544 | C=N stretching |
| 1276<br>1242<br>941 | C-$(CH_3)_3$ from *tert*-butyl groups |
| 1139<br>1036 | C-O stretching from ester groups |

## S4. Reaction setup for SI-O-ATRP of benzyl methacrylate

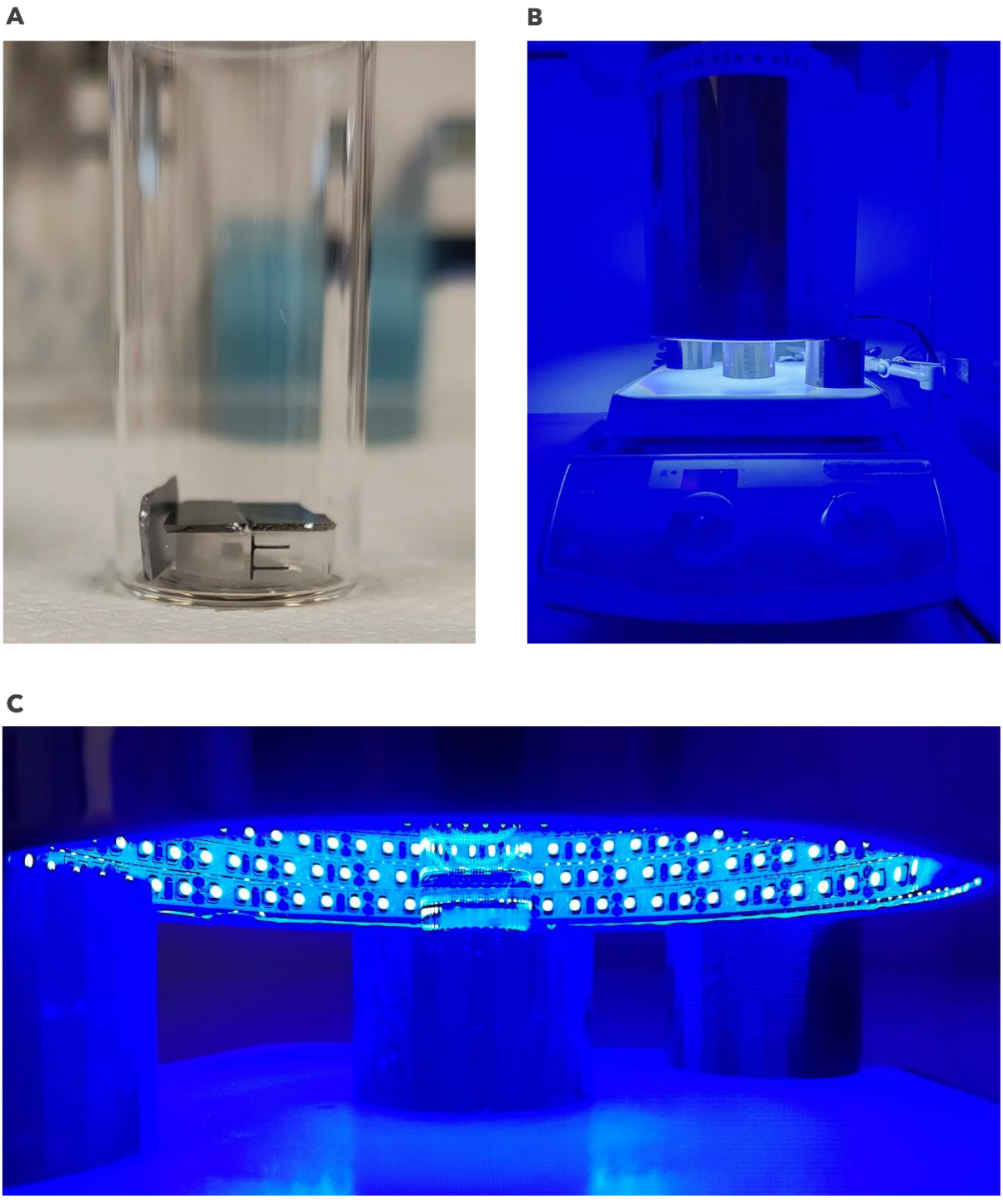


**Figure S11**. Photographs of experimental setup: **A** – initiator-functionalized silicon wafers placed in a custom-made holder; **B** – whole system with LED reactor ($\lambda_{max}$ = 450 nm) positioned on a magnetic stirrer; **C** – close-up view of the used platforms and position of polymerization mixture.

## S5. AFM characterization – kinetic studies of PBzMA brushes growth *via* SI-O-ATRP mediated by RF

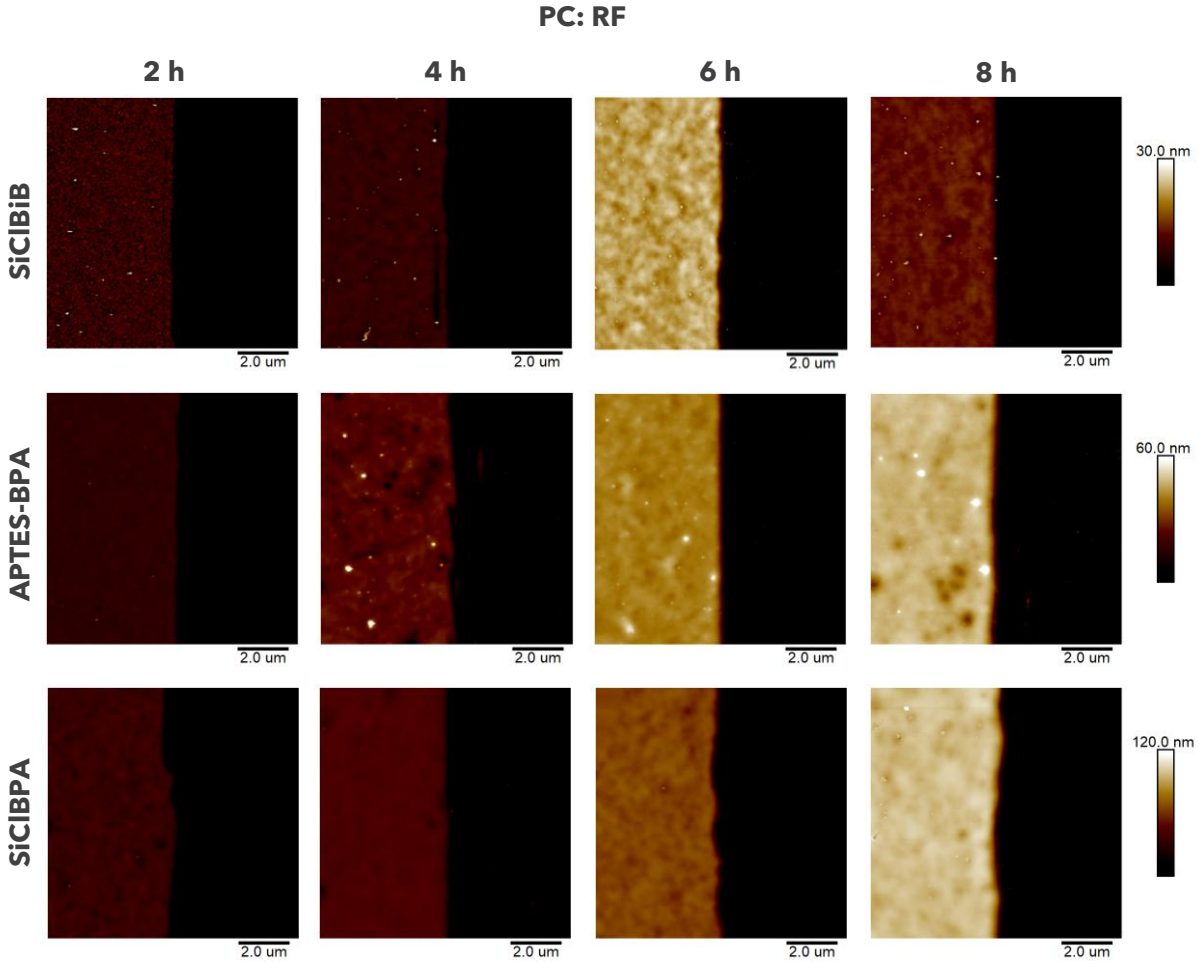


**Figure S12**. AFM topography images of PBzMA brushes synthesized on the silicon wafers functionalized with three types of surface initiators, after different times of SI-O-ATRP, under the conditions: 50/50 v/v BzMA/DMF; [BzMA]/[RF]: 1/0.000011 (11 ppm of RF); $V_{total}$ = 2 mL; $\lambda_{max}$ = 450 nm.

## S6. Characterization of PBzMA brushes after chain extension experiments

**Table S5**. Characteristics of samples subjected to chain extension experiments, obtained from different surface initiators in the following system: 50/50 v/v BzMA/DMF; [BzMA]/[**RF**]: **1/0.000011 (11 ppm of RF)**; $\lambda_{max}$ = 450 nm; $V_{total}$ = 2 mL.

| Time (h) | Initiator | Thickness of parent PBzMA brush (nm)[a)] | Thickness of PBzMa brush after chain extension (nm)[a)] |
|---|---|---|---|
| 8 + 8 | SiClBiB | 14 | 21 |
| 8 + 8 | APTES-BPA | 52 | 88 |
| 8 + 8 | SiClBPA | 107 | 160 |

[a)] *determined by VASE.*

## S7. Photophysical analysis of PC molecules

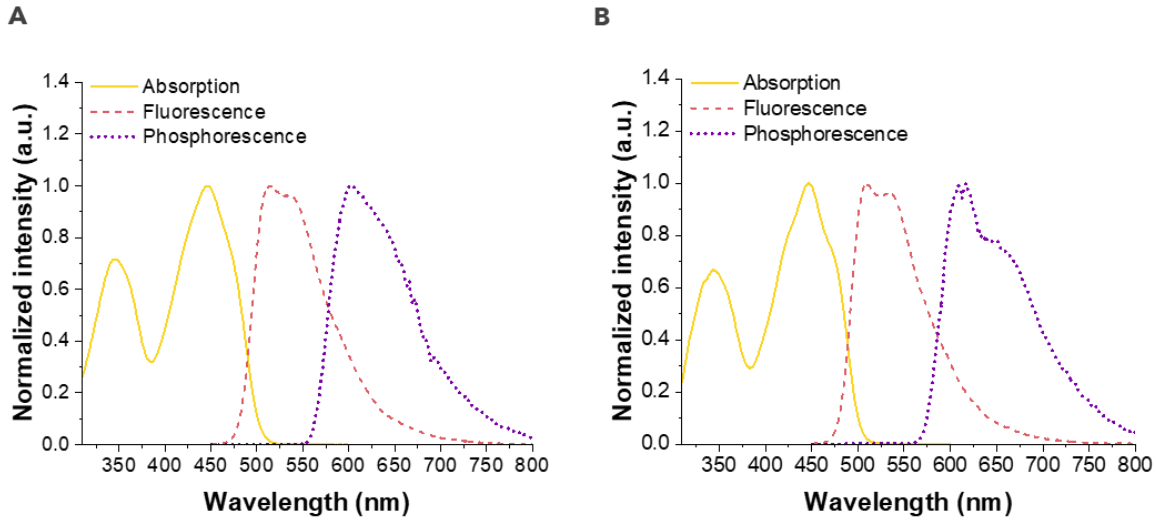


**Figure S13**. Normalized absorption, fluorescence and phosphorescence spectra of photocatalyst molecules in DMF: **A** – riboflavin; **B** – acylated riboflavin.

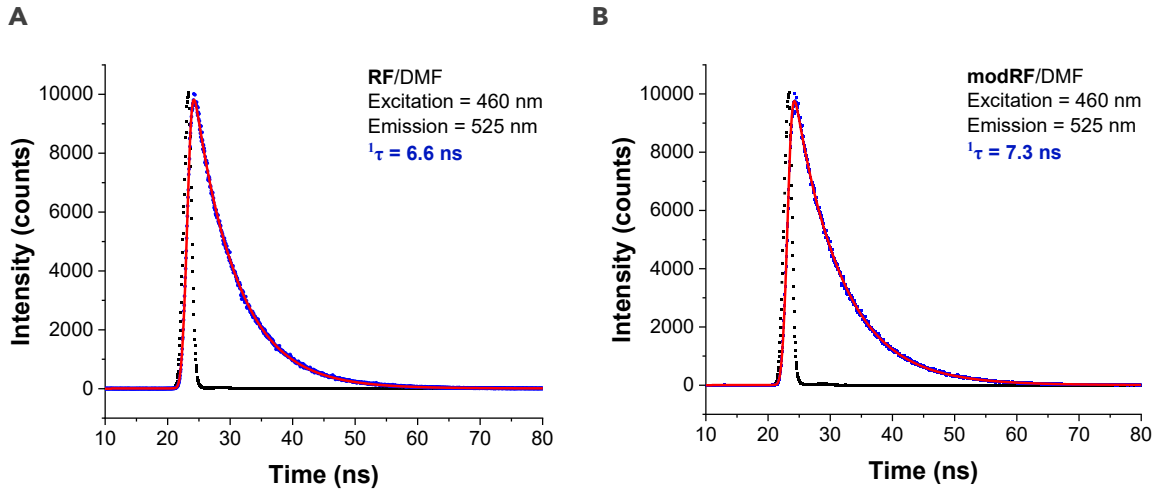


**Figure S14**. Emission decays recorded at 525 nm upon excitation at 460 nm for photocatalysts in DMF: **A** – riboflavin; **B** – acylated riboflavin; blue – experimental data, black – instruments response function, red – fit.

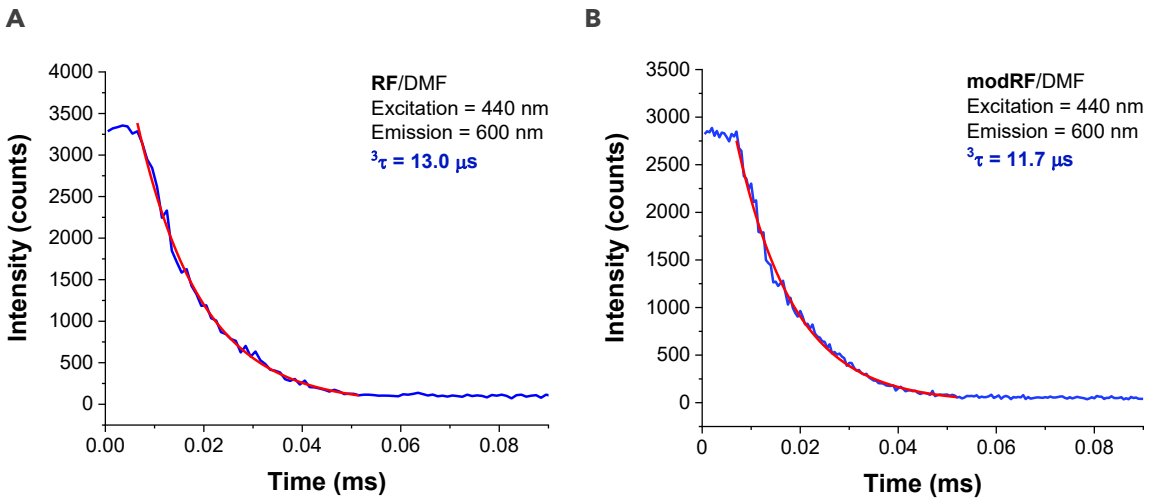


**Figure S15**. Emission decays recorded at 600 nm (at -196°C) upon excitation at 440 nm for photocatalysts in frozen DMF: **A** – riboflavin; **B** – acylated riboflavin; blue – experimental data, red – fit.

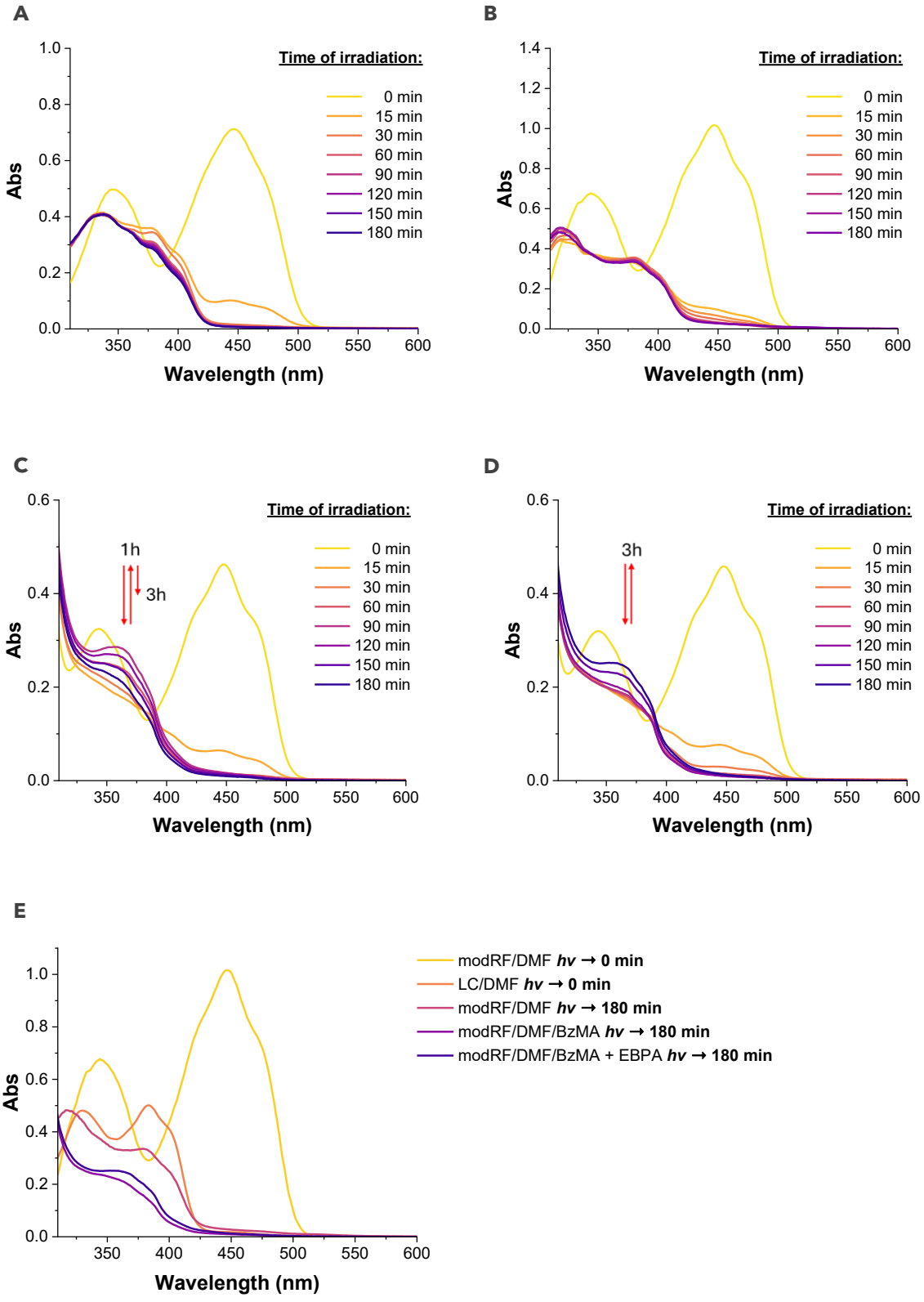


**Figure S16**. UV-Vis absorption spectra of photocatalyst molecules during irradiation at 450 nm: **A** – **RF** in DMF ($6.6 \times 10^{-5}$ M); **B** – **modRF** in DMF ($8.4 \times 10^{-5}$ M); **C** – polymerization mixture (50/50 v/v BzMA/DMF; [BzMA]/[**modRF**]: 1/0.000011 (11 ppm of modRF); **D** – polymerization mixture with the addition of 10 µL of 0.001 M EBPA/DMF stock solution; **E** – comparison of the selected spectra. Red arrows were added to highlight intensity fluctuations.

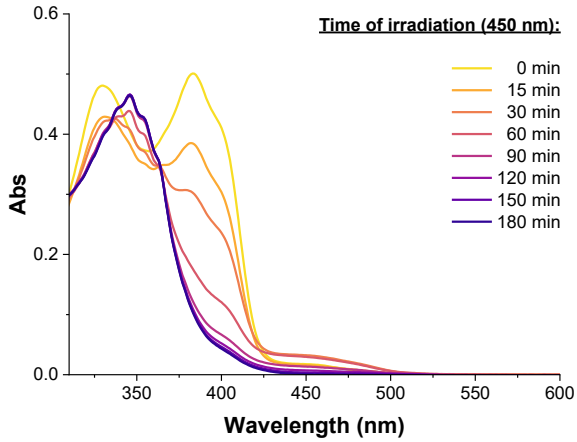


**Figure S17**. UV-Vis absorption spectra of lumichrome (LC) in DMF ($6.6 \times 10^{-5}$ M) during irradiation at 450 nm.

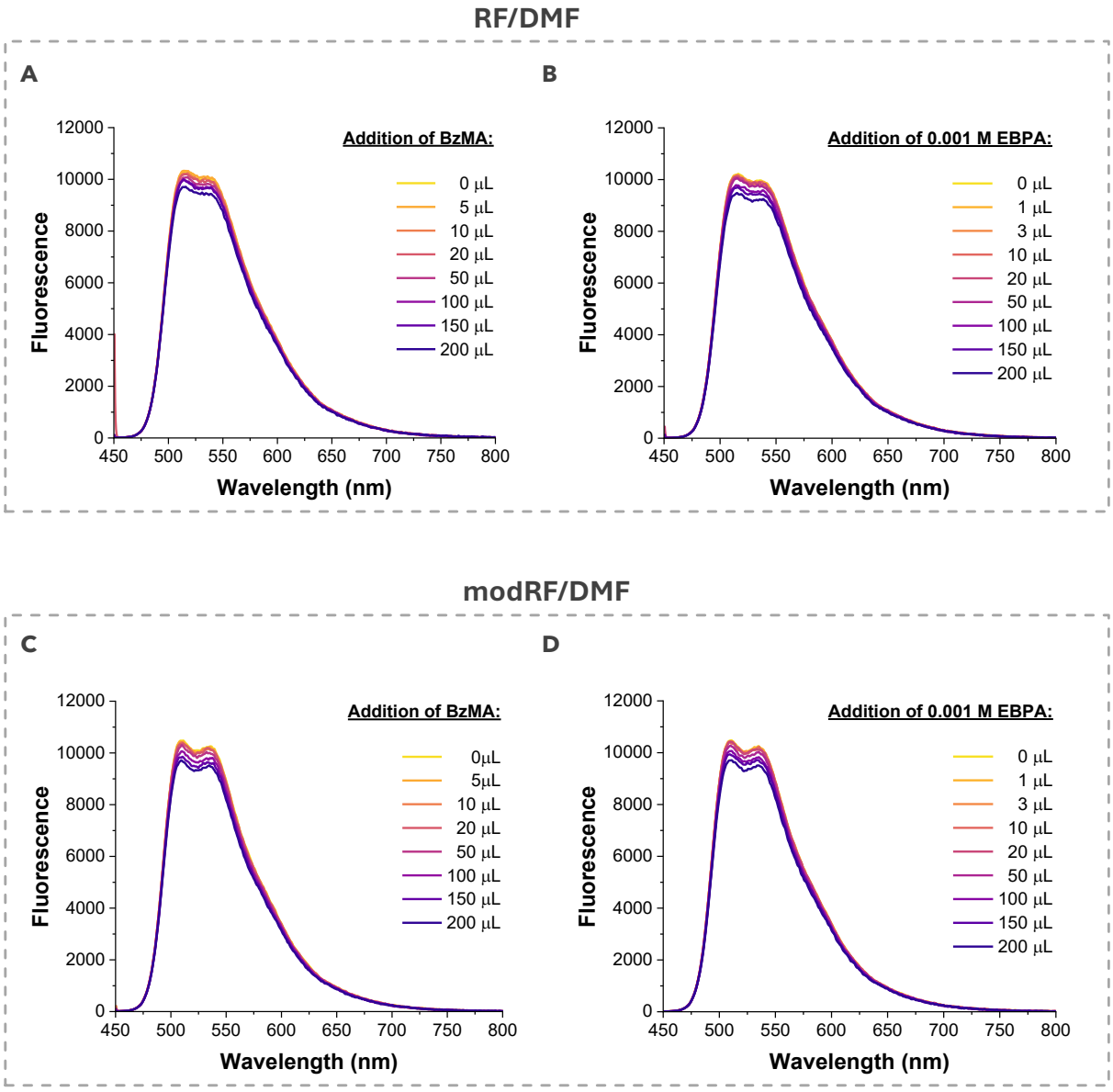


**Figure S18**. Fluorescence spectra of RF (**A** and **B**) and modRF (**C** and **D**) molecules in DMF ($1.7 \times 10^{-5}$ M) upon excitation at 440 nm: **A, C** – with the addition of 5 to a total of 200 µL of BzMA; **B, D** – with the addition of 1 to a total of 200 µL of 0.001 M EBPA/DMF stock solution.

**S8. AFM characterization – comparison of PBzMA brushes synthesized *via* SI-O-ATRP mediated by RF and modRF**

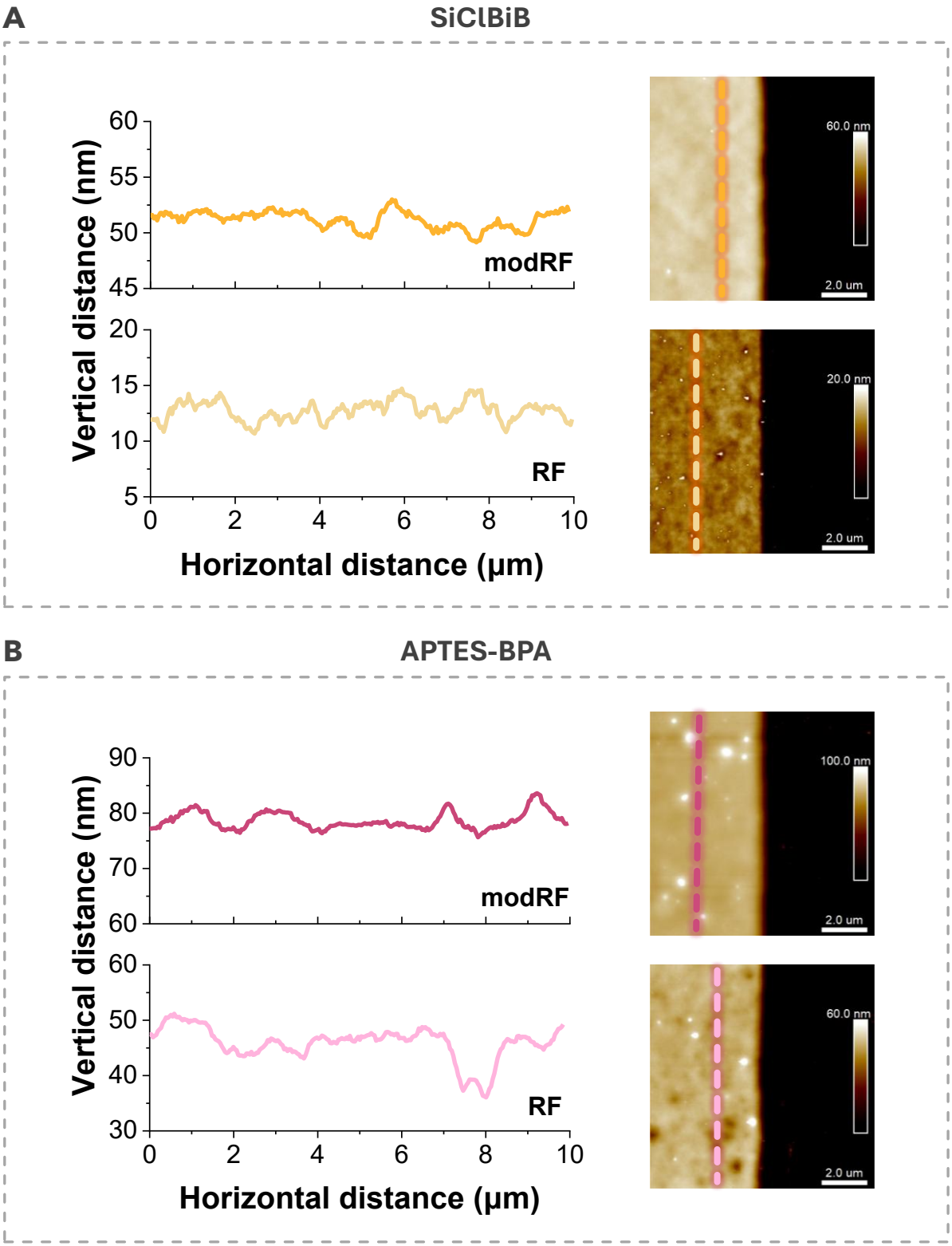

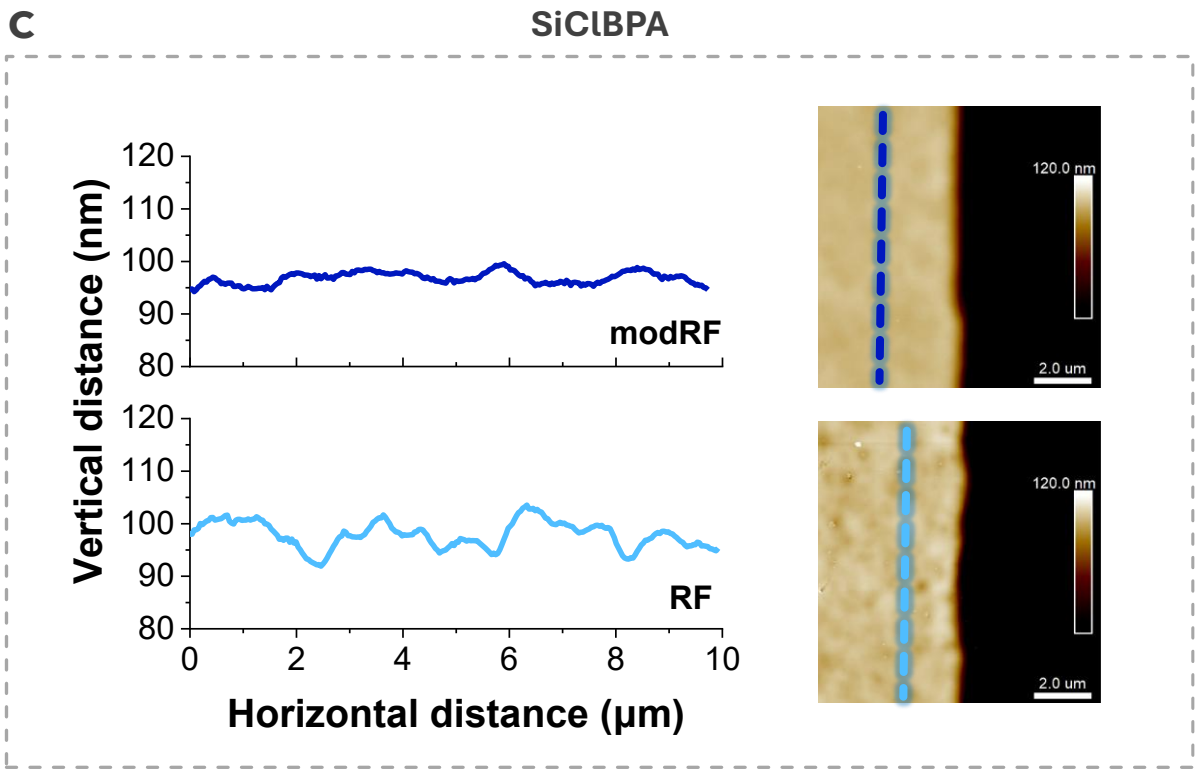


**Figure S19**. Topography profiles of PBzMA brushes with the corresponding AFM images showing the influence of PC structure on the roughness of the polymer layers synthesized from different ATRP initiators: **A** – SiClBiB; **B** – APTES-BPA; **C** – SiClBPA; experimental conditions: 50/50 v/v BzMA/DMF; [BzMA]/[PC]: 1/0.000011 (11 ppm of PC); $V_{total}$ = 2 mL; time: 8 h; $\lambda_{max}$ = 450 nm.

## S9. AFM characterization of PBzMA brushes synthesized *via* SI-O-ATRP mediated by LC

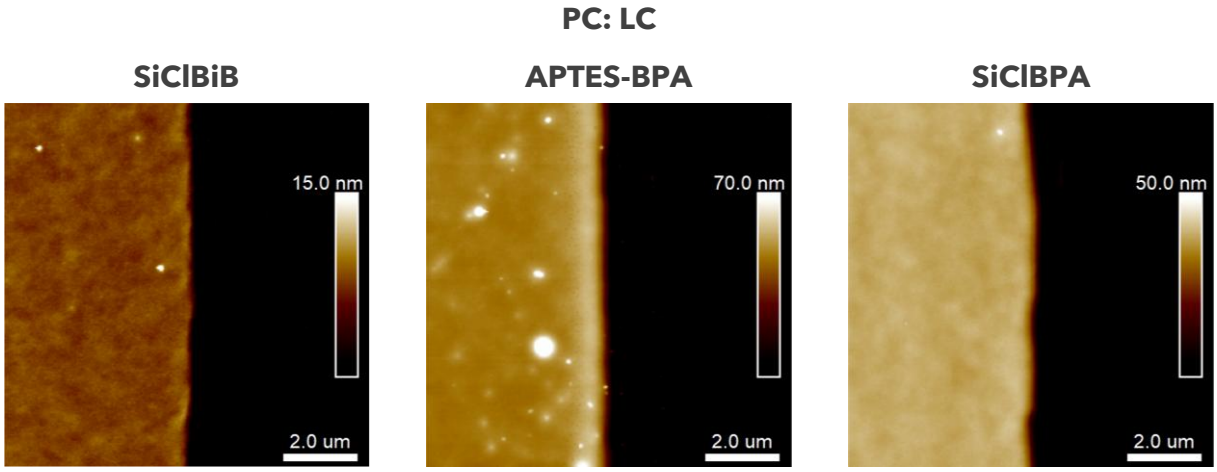


**Figure S20**. AFM topography images of PBzMA brushes synthesized on the silicon wafers functionalized with three types of surface initiators, under the conditions: 50/50 v/v BzMA/DMF; [BzMA]/[LC]: 1/0.000112 (112 ppm of LC); $V_{total}$ = 2 mL; time: 8 h; $\lambda_{max}$ = 450 nm.

## S10. AFM characterization – kinetic studies of PBzMA brushes growth *via* SI-O-ATRP mediated by modRF

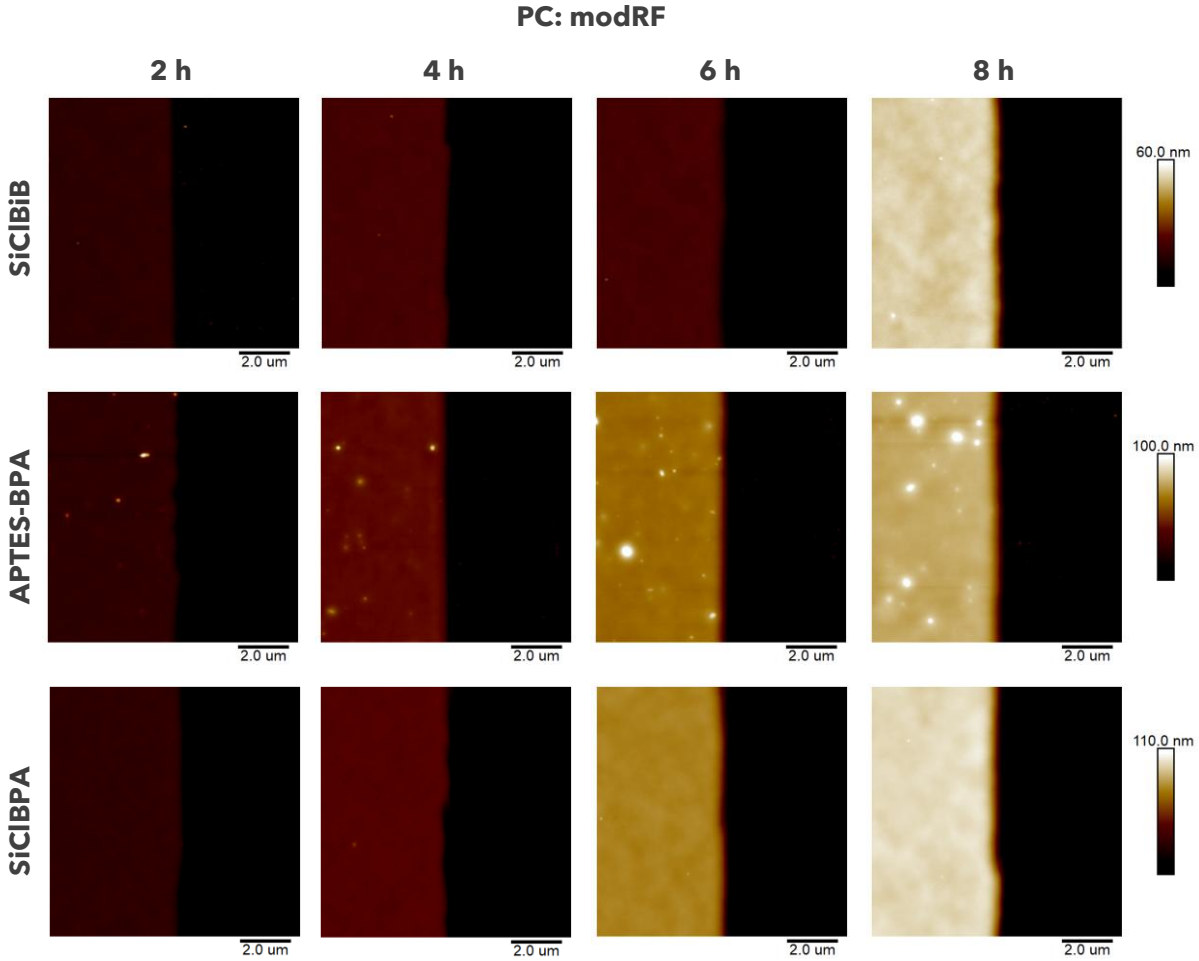


**Figure S21**. AFM topography images of PBzMA brushes synthesized on the silicon wafers functionalized with three types of surface initiators, after different times of SI-O-ATRP, under the conditions: 50/50 v/v BzMA/DMF; [BzMA]/[modRF]: 1/0.000011 (11 ppm of modRF); $V_{total}$ = 2 mL; $\lambda_{max}$ = 450 nm.

**Table S6**. Comparison of PBzMA brushes thickness obtained under slightly different experimental setups; experimental details: silicon wafer functionalized with SiClBPA initiator; 50/50 v/v BzMA/DMF; [BzMA]/[modRF]: 1/0.000011 (11 ppm of modRF); time: 4 h; $V_{total}$ = 2 mL; $\lambda_{max}$ = 450 nm.

| Entry | Constant stirring of polymerization solution | Deoxygenation | Thickness of PBzMA brushes (nm)[a)] |
|---|---|---|---|
| 1 | YES | YES | 44 |
| 2 | NO | YES | 21 |
| 3 | YES | NO | × |

[a)] *determined by VASE.*

## S11. Characterization of PBzMA brush used to determine the grafting density

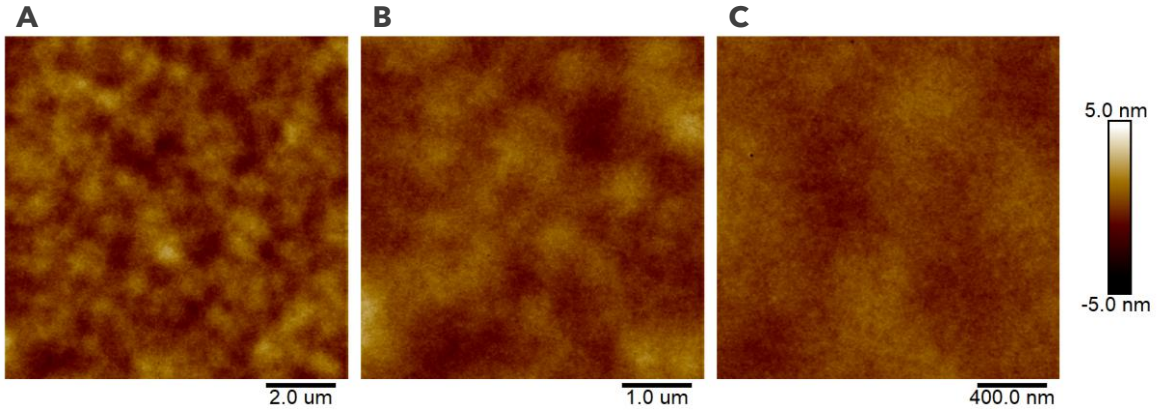


**Figure S22**. AFM topography images of PBzMA brush synthesized on the silicon wafer (Ø 10 cm) under the conditions: 50/50 v/v BzMA/DMF; [BzMA]/[modRF]: 1/0.000011 (11 ppm of modRF); time: 8 h; $V_{total}$ = 40 mL; $\lambda_{max}$ = 450 nm. **A** – scan size: 10×10 µm; **B** – scan size: 5×5 µm; **C** – scan size: 2×2 µm.

**Table S7**. Characteristics of sample subjected to degrafting experiment, obtained from large silicon wafer (Ø 10 cm) functionalized with SiClBPA initiator, in the following system: 50/50 v/v BzMA/DMF; [BzMA]/[modRF]: 1/0.000011 (11 ppm of modRF); time: 8 h; $V_{total}$ = 40 mL; $\lambda_{max}$ = 450 nm.

| Measurement point | Thickness of $SiO_2$ (nm)[a)] | Thickness of PBzMA brush (nm)[a) b)] | Thickness after PBzMA chains cleavage (nm)[a) b)] |
|---|---|---|---|
| 1 | 1.5 | 53.2 | -0.8 |
| 2 | 1.6 | 46.4 | -0.9 |
| 3 | 1.6 | 49.5 | -0.6 |
| 4 | 1.6 | 56.2 | -0.8 |
| 5 | 1.6 | 50.2 | 0.2 |

[a)] *determined by VASE;*

[b)] *$SiO_2$ layer thickness included in the multi-layer fitting model (Si/$SiO_2$/polymer layer).*

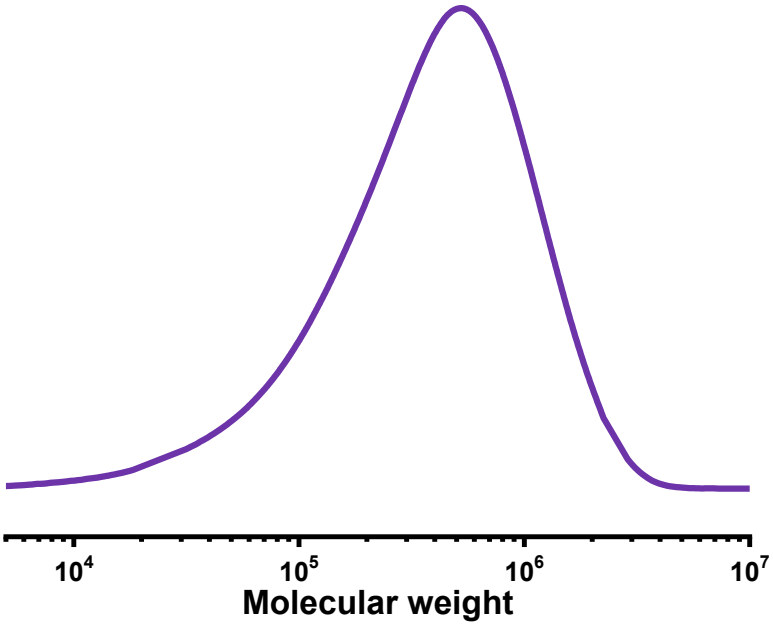


**Figure S23**. GPC trace of PBzMA generated in the solution during the synthesis of polymer brush on silicon wafer (Ø 10 cm) under the conditions: 50/50 v/v BzMA/DMF; [BzMA]/[modRF]: 1/0.000011 (11 ppm of modRF); time: 8 h; $V_{total}$ = 40 mL; $\lambda_{max}$ = 450 nm.

## S12. Kinetic studies of PBzMA O-ATRP in the solution

To gain a deeper understanding of the processes occurring during the O-ATRP mediated by RF or modRF, polymers synthesized in solution were analyzed. At first, we tested the EBiB ATRP initiator and various concentrations of modRF. Higher modRF concentration (625 ppm) leads to a slower monomer consumption compared to a low concentration (11 ppm). After 8 h of polymerization, the conversion reached 10% for high catalyst concentration and 28% when only 11 ppm of modRF was used. Both semi-logarithmic plots exhibited nearly linear characteristics, indicating a constant concentration of active centres during polymerization (**Figure S24**). This relationship correlates with the results obtained for the polymer brushes synthesis.

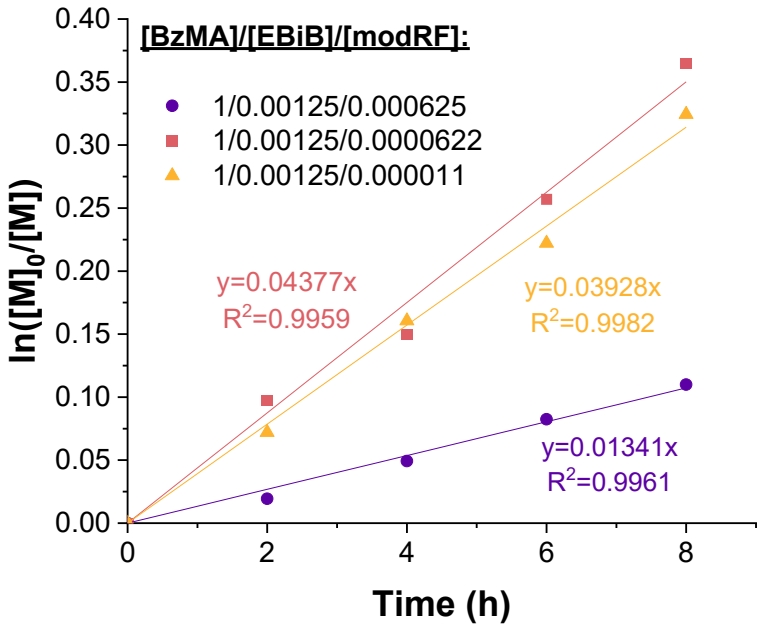


**Figure S24**. First-order kinetic plots of monomer conversion *vs.* polymerization time during PBzMA synthesis in the solution: purple plot – 50/50 v/v BzMA/DMF; [BzMA]/[EBiB]/[**modRF**]: 1/0.00125/**0.000625** (625 ppm of modRF); red plot – 50/50 v/v BzMA/DMF; [BzMA]/[EBiB]/[**modRF**]: 1/0.00125/**0.0000622** (62 ppm of modRF); yellow plot – 50/50 v/v BzMA/DMF; [BzMA]/[EBiB]/[**modRF**]: 1/0.00125/**0.000011** (11 ppm of modRF).

In order to verify whether ATRP initiator structure plays an important role in the polymerization in solution, we attempted O-ATRP utilizing [BzMA]/[initiator]/[modRF] system: 1/0.00125/0.0000622 (62 ppm modRF), and sacrificial initiators structurally similar to those tested in polymer brush synthesis: EBiB and EBPA. Results are provided in **Table S8**.

**Table S8**. Influence of ATRP initiator on the PBzMA synthesis in the solution: 50/50 v/v BzMA/DMF; [BzMA]/[initiator]/[**modRF**]: 1/0.00125/**0.0000622** (62 ppm of modRF).

| Entry | Initiator | Time (h) | Conv[a] (%) | $I_{eff}$[b] (%) | $M_{n,theo}$[c] (× $10^3$ g $mol^{-1}$) | $M_{n,app}$[d] (× $10^3$ g $mol^{-1}$) | Đ[d] |
|---|---|---|---|---|---|---|---|
| **1** | EBiB | 24 | 33 | 37 | 47 | 129 | 2.8 |
| **2** | EBPA | 24 | 99 | 111 | 140 | 125 | 3.1 |

[a] *Monomer conversion was determined by $^1H$ NMR;*

[b] *Initiation efficiency, $I_{eff} = (M_{n,theo}/M_{n,app}) \times 100\%$;*

[c] *$M_{n,theo} = ([BzMA]_0/[initiator]_0) \times conversion \times M_{BzMA} + M_{initiator}$;*

[d] *Apparent $M_{n,app}$ and Đ were determined by GPC.*

In the case of the EBiB initiator, a gradual increase in molecular weight is observed alongside monomer conversion, which reaches 33% after 24 h (**Figure S25**). However, the dispersity remains high (Đ > 2.5), while semilogarithmic plot indicates substantial termination and decreasing concentration of active centres after 8 h. It indicates insufficient control of O-ATRP in the solution under applied conditions. The kinetic graph for the EBPA initiator reveals an induction period with an increase in active centres over time, ultimately achieving nearly 100% monomer conversion after 24 h (**Figure S26**). On the one hand, it indicates the greater involvement of EBPA molecules in the production of active propagating canters, but on the other hand, the initiation process is slow, leading to the formation of polymer chains with a much broader molar mass distribution (Đ = 2.2-3.3) compared to surface-grafted chains. The lower reactivity of the EBiB initiator corresponds to a low initiation efficiency ($I_{eff}$), which can be estimated to 37% after 24 h. In contrast, the EBPA initiator shows a clear increase in $I_{eff}$ to 111% (monomer conversion ≈ 100%, 24 h), indicating the participation of additional initiation sites beyond the ATRP mechanism. It is worth mentioning that we were focused in this work on optimization of SI-O-ATRP conditions in which the concentration of initiating species attached to the surface is much lower (can be estimated to up to a few nanomoles) compared to O-ATRP in the solution (3-4 orders of magnitude greater amount of free initiators). Therefore, the concentration of PC can be too small to effectively control this process. Another problem in the case of O-ATRP in the solution is the fact that active centres can be generated not only from the alkyl halides but also directly from the PC molecule, whose rich electronic structure contains sites capable of freely generating radicals, such as the nitrogen atoms within the isoalloxazine ring. If the polymerization is initiated from multiple species, this may contribute to the high dispersity values. These side processes are not that important in the case of polymer brush synthesis, since the only source of active centres in the case of surface-grafted chains is

alkyl halides participating in the ATRP equilibrium. Therefore, the developed synthetic conditions of SI-O-ATRP are useful rather for the synthesis of polymer brushes enabling the production of well-defined polymer layers utilizing naturally derived PC and a quite simple reaction setup.

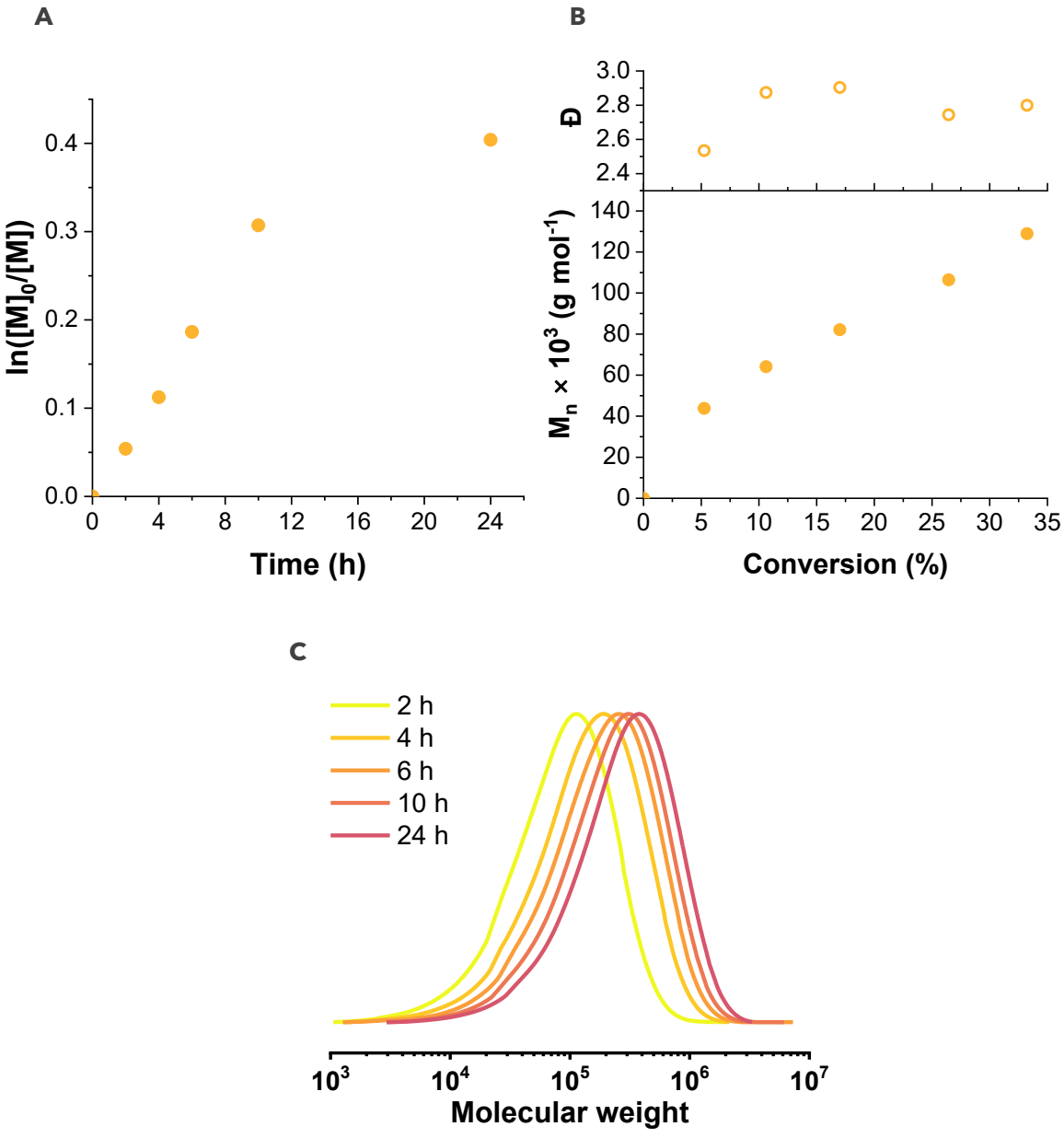


**Figure S25**. Characterization of PBzMA chains obtained in the solution: [BzMA]/[**EBiB**]/[modRF]: 1/0.00125/0.0000622 (62 ppm modRF): **A** – first-order kinetic plot of monomer conversion *vs.* polymerization time; **B** – $\mathbf{M_n}$ and **Đ** *vs.* monomer conversion; **C** – GPC traces of the obtained polymers.

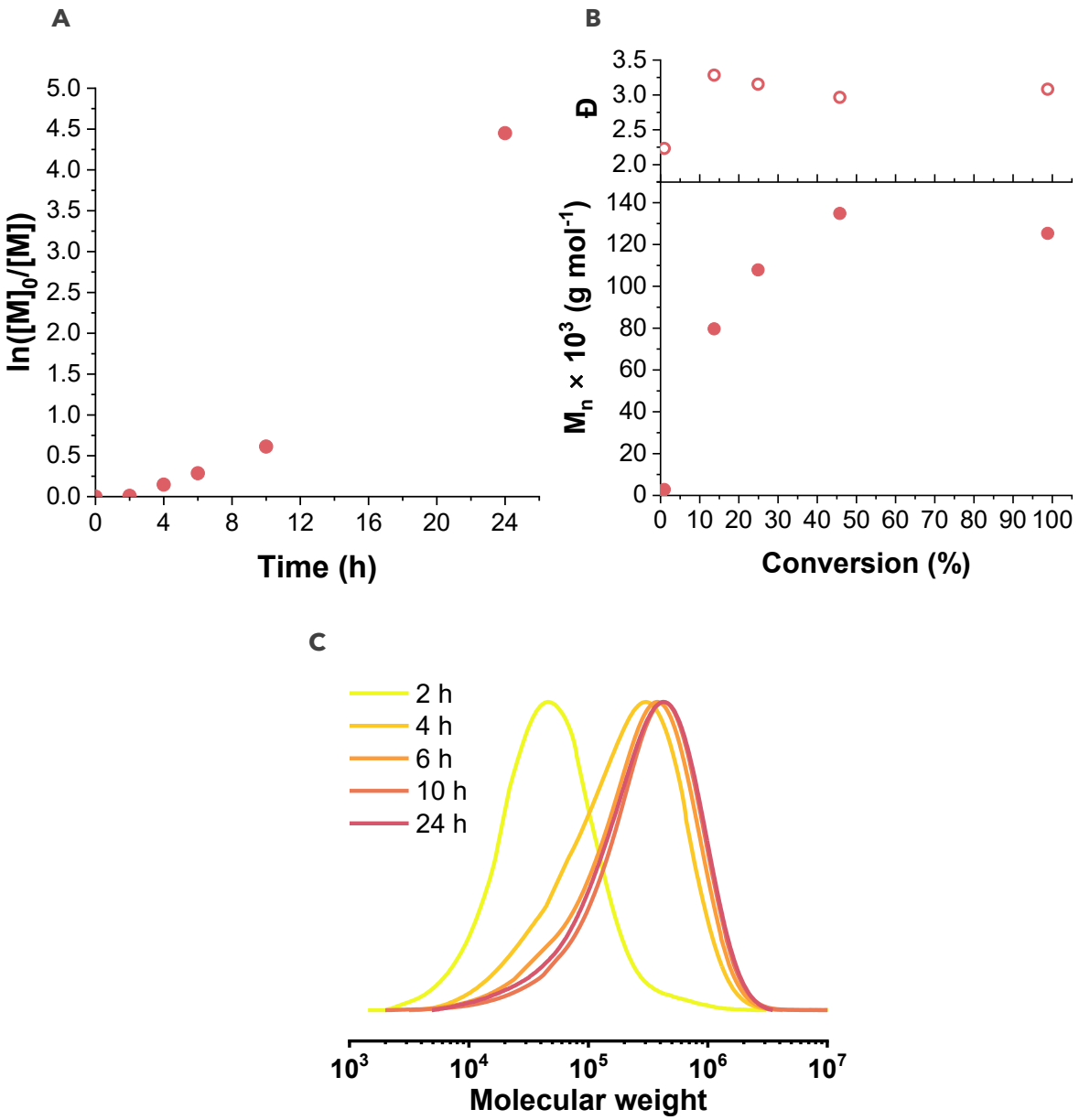


**Figure S26**. Characterization of PBzMA chains obtained in the solution: [BzMA]/[**EBPA**]/[modRF]: 1/0.00125/0.0000622 (62 ppm modRF): **A** – first-order kinetic plot of monomer conversion *vs.* polymerization time; **B** – $\mathbf{M_n}$ and **Đ** *vs.* monomer conversion; **C** – GPC traces of the obtained polymers.

## References


1 J. Yan, X. Pan, M. Schmitt, Z. Wang, M. R. Bockstaller and K. Matyjaszewski, *ACS Macro Lett.*, 2016, **5**, 661–665.

2 I. Zaborniak, K. Surmacz, M. Flejszar and P. Chmielarz, *J. Appl. Polym. Sci.*, 2020, **137**, 49275.

3 J. R. Lakowicz, *Principles of fluorescence spectroscopy*, Springer US, Boston, MA, Third Edit., 2006.

4 J. Kozioł and E. Knobloch, *Biochim. Biophys. Acta (BBA)-Biophys. Incl. Photosynth.*, 1965, **102**, 289–300.

5 J. Smenda, K. Wolski, K. Chajec and S. Zapotoczny, *Polymers*, 2021, **13**, 4458.

6 A. Kiełbasa and K. Wolski, *Eur. Polym. J.*, 2025, **233**, 113961.

7 J. Wang and H. A. Klok, *Angew. Chem. Int. Ed.*, 2019, **58**, 9989–9993.